J. Fluid Mech. (1985), *vol.* 151, *pp.* 395–426
Printed in Great Britain

Observation of waves during oscillatory channel flow

By IAN J. SOBEY†
School of Mathematics, University of Bristol, Bristol B58 1TW, England

(Received 6 March 1984)

We have observed steady and oscillatory flow through a two-dimensional channel expansion. The experimental results are supported by numerical solutions of the unsteady Navier–Stokes equations. This work was prompted by the recent discovery of vortex waves during steady flow past a moving indentation in a channel wall. Our work deals with both asymmetric channels, in which we show that vortex waves are observed during oscillatory flow with rigid walls, and with symmetric channels, in which a vortex street is observed. We believe that the vortex street is not a vortex wave, but the result of a shear-layer instability.

1. Introduction

It has recently been observed that during steady flow through a two-dimensional channel a wave can be produced downstream of a moving indentation (Stephanoff *et al.* 1983, hereinafter referred to as I). The wave has the form of a series of vortices alternating on the walls of the channel with the mainstream following a sinuous path between the vortices. The existence of a wave in these circumstances seems to have been first indicated by Secomb (1979) who derived a linearized Korteweg–de Vries equation to describe the motion in the core of the channel for very small amplitude wall indentations. It was not realized at that time that a wave of vortices could be produced. Bertram & Pedley (1982) observed impulsively started flow past a fixed channel expansion, concentrating mainly on the separated region which occurred in the lee of the expansion. Without realizing it then, they also observed a wave of vortices (their figure 10) but attributed them to be a vortex 'street' due to 'the quasi-steady instability of a velocity profile with an inflexion point'. The reason for the wave of vortices may have been an oscillation in the flux through the channel (such oscillations are indicated by their figure 19). Ryzhov & Zhuk (1980), Terentev (1981) and Bogdanova & Ryzhov (1983) have concentrated on the free interaction wall layers which occur during steady flow past very small amplitude wall oscillations. They have shown that the boundary-layer equations they derive can support a wavelike solution downstream of the section of moving wall and, most importantly, the wave becomes neutrally damped as the frequency of the oscillation approaches a critical value. They also have not suggested that the wavelike structure could produce a wave of vortices. The wave reported in I appears to be a new form of wave motion. As we have shown, it was unexpected and as yet has no complete analytic description. The model proposed in I, which is an extension of the work of Secomb (1979), does explain some of the observed features of the wave. We propose to call the wave of vortices and the associated wavy core flow a vortex wave.

In this paper we present experimental observations of both steady and unsteady

† Present address: Schlumberger Cambridge Research, P.O. Box 153, Cambridge CB2 3BE, England.

two-dimensional flow through a rigid walled channel. Our observations are supported by numerical solutions of the unsteady Navier–Stokes equations. We find that a vortex wave is generated by oscillatory flow in an asymmetric channel. During oscillatory flow in a symmetric channel we have observed an asymmetric disturbance which results in a wave but we believe that this is an example of a vortex street and results from a shear-layer instability.

Currently there is considerable interest in both steady and unsteady separation in two-dimensional channels. Using a multiple deck analysis Smith (1976*a*, *b*) considered steady flow through a slightly distorted channel. That work has been extended by Smith (1977) and Smith & Duck (1980) who have considered larger disturbances. In symmetric channels they found that the core should remain undisturbed. It is well known that, whilst this is true for small Reynolds numbers, it does not happen for larger Reynolds numbers when the symmetric flow is unstable and a bifurcation phenomenon occurs. In unsteady flow there is as yet no comprehensive asymptotic description of the flow, although Cowley (1981) has considered some aspects of a flow driven by an unsteady pressure gradient. One point worth mentioning is that the experiments and calculations described below are for large channel distortion and moderate Reynolds number, whereas the theories referred to are for very small channel distortion and asymptotically large Reynolds number. It might be thought that these represent two extremes which should not be expected to be related. We do not agree since Sobey's (1980) calculation of solutions to the full Navier–Stokes equations showed very close agreement to the asymptotic theory of Smith (1976*a*) at a Reynolds number of 75.

There exists a considerable number of observations of steady flow through a channel expansion. Flow over a back-facing step can be found in Goldstein *et al.* (1970), Denham & Patrick (1974) and Armaly *et al.* (1983). Recent observations of flow through a symmetric channel are given by Durst, Melling & Whitelaw (1974), Cherdron, Durst & Whitelaw (1978) and John (1984). The main results are that in an asymmetric channel the length of the separated region increases linearly with Reynolds number, and that in a symmetric channel the symmetric flow becomes unstable at a Reynolds number which depends on the expansion ratio: for a 1:3 expansion the critical Reynolds number lies in the range 20–40 depending on the aspect ratio of the channel. Above that Reynolds number a steady asymmetric flow can be observed. The flow is usually explained by a 'Coanda' effect whereby the flow attached to one wall has a high velocity, and thus a low pressure, and so the asymmetric flow can be maintained by the cross-channel pressure gradient.

There are two fluid-dynamic parameters which characterize an oscillatory flow: the Reynolds and Strouhal numbers. If the minimum channel half gap is h, the flux $2hU$, frequency Ω and viscosity ν then we define

$$Re = \frac{hU}{\nu} \quad \text{and} \quad St = \frac{h\Omega}{U}.$$

In steady flow the Strouhal number vanishes. In both steady and unsteady flow if the Reynolds number is small ($Re = O(1)$) the flow is dominated by viscosity and separation does not occur. In the case of oscillatory flow if the Strouhal number is large ($St = O(1)$) the flow is again dominated by unsteady inertia and viscosity (Sobey 1980). At moderate Reynolds number ($Re = O(10–100)$) and smaller Strouhal number, convective inertial effects are important and separation can occur. At very small Strouhal number ($St = O(10^{-4})$) separation is quasi-steady whilst at intermediate Strouhal number ($St = O(0.01–0.001)$) separation is not quasi-steady and the main effect observed is the expansion of vortices during the deceleration (Sobey 1983). As yet there are no asymptotic studies which are valid at intermediate Strouhal number but the numerical solution of the unsteady interactive boundary-layer equations by Duck (1984) and Cowley & Tutty (private communication) may allow a detailed understanding of the nonlinear effects which are observed to occur in these flows.

In this paper we describe in §2 the details of our experimental apparatus and then present in §§3 and 4 our observations of steady and unsteady flow through symmetric and asymmetric channels. In §5 we give numerical solutions of the Navier–Stokes equations which support the observations. Finally, in §6 we present a discussion of the results and compare them with the existing literature.

2. Experimental apparatus

We have observed steady and oscillatory flow in a rectangular channel in a purpose-built rig. The apparatus is shown schematically in figure 1. A recirculating pump allowed a pressure head to drive steady flow. The flow rate was calculated using a measuring cylinder and a stop watch, and a calibration curve was derived for pressure head versus flow rate. Oscillatory flow was generated using a rolling diaphragm pump driven by a variable-speed motor and adjustable crankshaft. This produced approximately sinusoidal fluxes, the deviation in our rig being less than 2% throughout the cycle. Channels were machined from Perspex and their interior dimensions were 155 mm length, 15 mm width and with channel gaps which varied between 1 and 3 mm. The aspect ratio of the channels varied between 15:1 and 5:1 and approximately two-dimensional flow could be observed across the centreplane of the channel. At the entrance to each channel was a 10 mm diffuser followed by a section 28 mm long and with a constant 1 mm gap, used as a flow straightener before the channel changed cross-section. A typical channel is illustrated in figure 2. Two geometries were studied in detail: a right-angled expansion and a 45 expansion. In each case the expansion was 1 mm. Interchangeable sections allowed both asymmetric (1 mm channel gap becoming 2 mm) and symmetric (1–3 mm gap) expansions to be observed.

If the piston area is A_p, the total piston displacement k(mm) and the motor frequency Ω(Hz), then the instantaneous piston displacement can be written

$$\tfrac{1}{2}k(1-\cos 2\pi\Omega t),$$

where t is the dimensional time. The piston velocity is then

$$k\pi\Omega \sin 2\pi\Omega t,$$

and hence the flux through the channel is

$$k\pi\Omega A_p \sin 2\pi\Omega t.$$

If the channel width is w(mm) and minimum gap is $2h$(mm), the velocity scale is

$$U=\frac{\pi k\Omega A_p}{2hW},$$

and the two governing parameters are

$$Re=\frac{\pi k\Omega A_p}{2w\nu} \quad \text{and} \quad St=\frac{2h^2w}{\pi A_p k}.$$

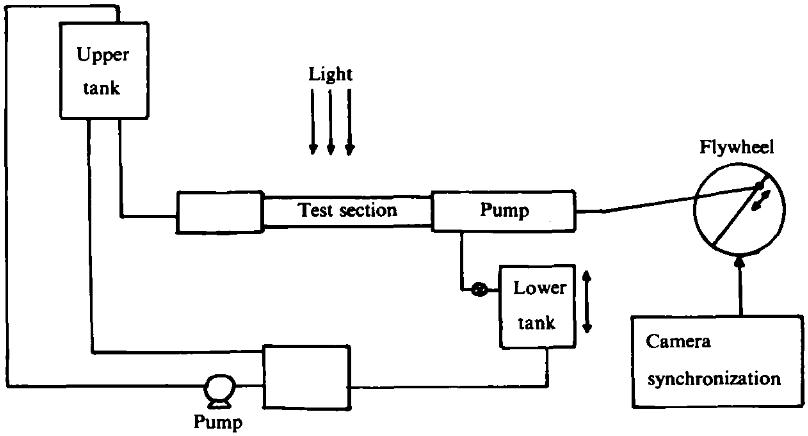

FIGURE 1. Schematic diagram of experimental apparatus.

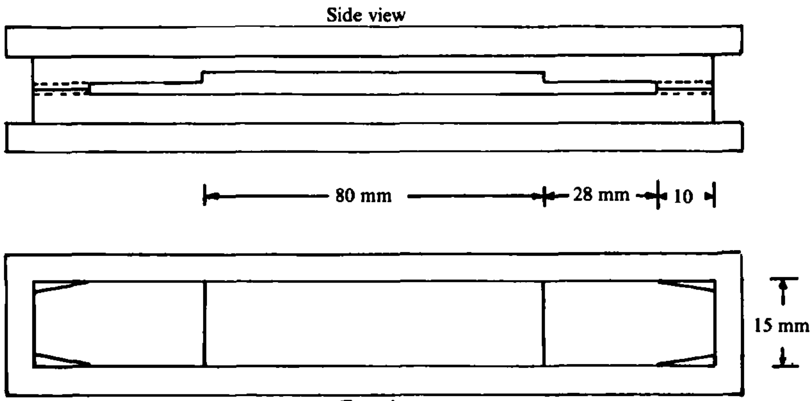

FIGURE 2. Details of channel geometry.

Note that the Strouhal number, which in the Navier–Stokes equations distinguishes the unsteady term from the nonlinear inertial terms, is dependent only on the piston displacement. It is the ratio of the channel lengthscale to the scale of a fluid particle's displacement. In our experiments the piston area was 198 mm^2 and the observations were carried out in water with viscosity approximately 1 $\mathrm{mm}^2/\mathrm{sec}$ giving

$$Re = 20.7k\Omega \quad \text{and} \quad St = 0.012k^{-1}.$$

The frequency Ω was continuously variable between 0.5 and 2.5 Hz and the piston displacement had a working range 0.5–10 mm. Thus the parameter range we could observe was $0.0012 < St < 0.24$ and $5 < Re < 500$. In practice the flow became unstable at Reynolds numbers above 200 and our experiments were confined to the lower end of the Reynolds number range.

For steady flow the pressure head could be varied between 25 and 100 mm water producing a Reynolds number range $7 < Re < 125$. A separate calibration was carried out for each channel.

Flow visualization was by means of small reflective particles (Mearlmaid AA, The Mearl Corp., N.Y.) illuminated by a 250 W slide projector. Still photographs were taken with a motor-driven Nikon camera and ASA400 film (Kodak Tri-X, Ilford

HP5). For steady flow, exposures varied between $f8$ at $\frac{1}{8}$ s and $f22$ at 4 s, whilst for unsteady flow we used $f5.6$ at $\frac{1}{60}$ s. The photography was synchronized by a variable-position take-off from the flywheel allowing 80 ms delay on the motor drive unit.

3. Steady flow

3.1. *Asymmetric channels*

We have observed flow past an asymmetric right angled expansion and those results are shown in figure 3. At a Reynolds number of 7 a small recirculating region existed in the corner. As the Reynolds number was increased to 115 the vortex rapidly grew in size and strength. The form was very elongated, showing that the vortex was driven by the shear layer present at the sudden expansion. On the opposite wall there was no evidence of a vortex but a wall layer was clearly evident slightly downstream of the vortex (see figures 3(*c*) and (*d*) particularly). The wall layer showed that there was a region of significantly reduced shear on the opposite wall in accordance with the theory of Smith (1976*a*). Armaly *et al.* (1983), whose Reynolds numbers are four times ours, have observed a vortex on the opposite wall at Reynolds numbers above 100. We have measured from the photographs the distance from the expansion to the reattachment point. The measurements were made by visually estimating where reattachment occurred and, as shown in figure 4, there was an approximately linear increase in vortex length as the Reynolds number was varied over the range of our experiments, given by $L_s = 2+0.13Re$. The data of Armaly *et al.* agrees well with this, our interpretation of their figure 13(*a*) giving $L_s = 2+0.14Re$.

3.2. *Symmetric channels*

When flow occurs past a symmetric expansion then we would expect separation to occur on each wall. At a small Reynolds number (figure 5*a*) a small separated region existed on each wall and was larger than that observed at the same Reynolds number in an asymmetric channel. The vortices were symmetric at that stage but as the Reynolds number increased to near 25 the flow became asymmetric and one vortex began to grow whilst the other at first became smaller and then remained of constant length. In our experiments the dominant vortex could appear on either wall although there was a marked predilection for it to appear on one wall only. If, as expected, the asymmetric behaviour was caused by an instability of flow in the presence of symmetric vortices then small local asymmetries may have triggered the instability in one direction most of the time. If the Reynolds number was increased further the flow became three-dimensional and ultimately an unsteady instability occurred which caused the mainstream to oscillate slowly from side to side. This instability was well established when the Reynolds number was 165 (figure 5*d*).

In an attempt to investigate the assumption of two-dimensional flow in the centreplane we observed the particles from the side of the channel. Those results are also shown in figure 5 together with the corresponding flow observed in the centreplane of the channel. At a small Reynolds number the flow is approximately two-dimensional for most of the width of the channel with only small three-dimensional vortices in the corners. As the Reynolds number was increased the three-dimensional vortices grew although the flow at the centre of the channel remained two-dimensional. This remained true until about a Reynolds number of 70 when the entire flow became three-dimensional and the line of attachment sloped at a considerable angle to the channel (figure 5*g*). Note that there were still two three-dimensional vortices but the lower one in the photograph had grown to dominate the flow. If the Reynolds number

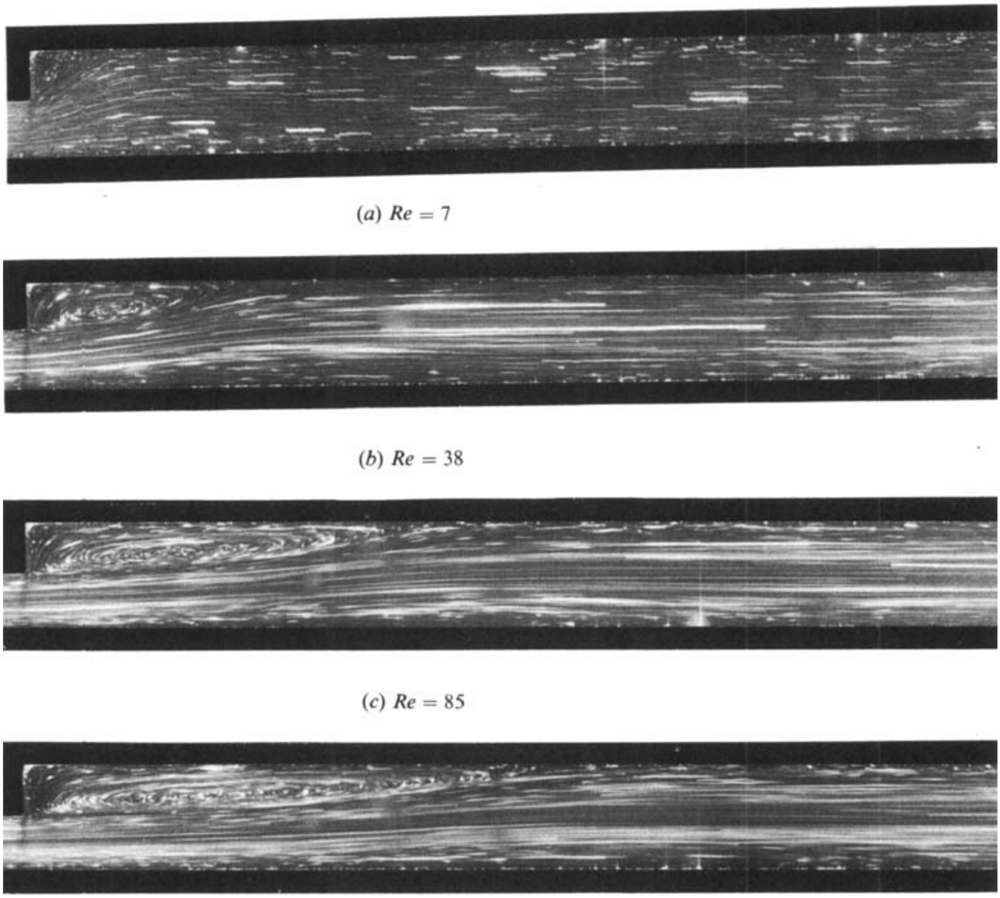

(a) $Re = 7$

(b) $Re = 38$

(c) $Re = 85$

(d) $Re = 115$

FIGURE 3. Steady flow through an asymmetric expansion: (a) $Re = 7$, (b) $Re = 38$, (c) $Re = 85$, (d) $Re = 115$.

was increased further the three-dimensional vortices at first increased in size but then lost their structure as the flow became unsteady (figure 5h). These results showed that although the symmetric flow was unstable the asymmetric flow that resulted was stable and remained two-dimensional for a considerable range of Reynolds number.

If, instead of a right-angled expansion, the channel walls were sloped at an angle of 45° then a similar pattern was still observed and is shown in figure 6. As the Reynolds number was increased the flow, which was initially symmetric, became asymmetric and then three-dimensional and unsteady, as can be seen from the criss-cross pattern of particle paths in figure 6(d).

The length of the separated regions were measured from the photographs and are shown in figure 7 for both channels. In each case the instability became apparent at a Reynolds number of approximately 25 and thereafter one vortex increased linearly with Reynolds number whilst the other at first decreased in length and then remained of constant size. In each channel, as the Reynolds number increased, the sequence of events was as follows. A steady two-dimensional symmetric flow became

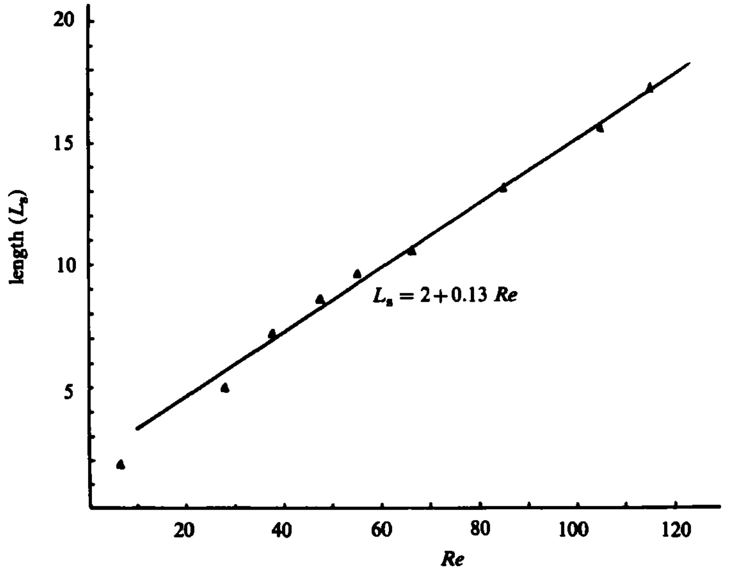

FIGURE 4. Variation of vortex length (L_S) with Reynolds number for an asymmetric channel.

a steady two-dimensional asymmetric flow and this was followed by a steady three-dimensional asymmetric flow. Thereafter an unsteady asymmetric flow developed and eventually a three-dimensional turbulent flow existed.

4. Oscillatory flow

4.1. *Asymmetric channels*

We report here the bulk of our observations which show that in an oscillatory flow a wave of vortices can be generated by a change in the channel geometry. The wave consists of a series of separated regions, generally alternating on the two walls and with the mainstream flowing in a wavy path between the vortices. The flow remained two-dimensional and laminar at small Reynolds numbers but became three-dimensional and intermittently turbulent at larger Reynolds number. Both the Reynolds number and the Strouhal number had a strong influence on the observed flow patterns. We defer until later any discussion of the significance or genesis of the vortex wave and restrict ourselves here to a description of our observations.

Firstly, we show in figure 8 the typical flow patterns observed during a cycle. These patterns are at a Reynolds number of 80 and Strouhal number of 0.003, approximately the mid-point of the region in parameter space in which we could make observations. At peak flow, figure 8 (*a*), separation has occurred in the lee of the channel expansion forming what we shall refer to as the primary vortex, together with a strong secondary vortex attached to the opposite wall. The centre of the primary vortex was further downstream than in the case of steady flow and the secondary vortex was a consequence of the unsteady nature of the flow, since it was not observed during steady flow. As the fluid flux was decreased there was a general deceleration of the flow, expressed by an adverse pressure gradient throughout the channel. At this stage there was an expansion of the vortices, although note that in figure 8 (*b*) the secondary vortex has become smaller and moved upstream some distance, and it was only after

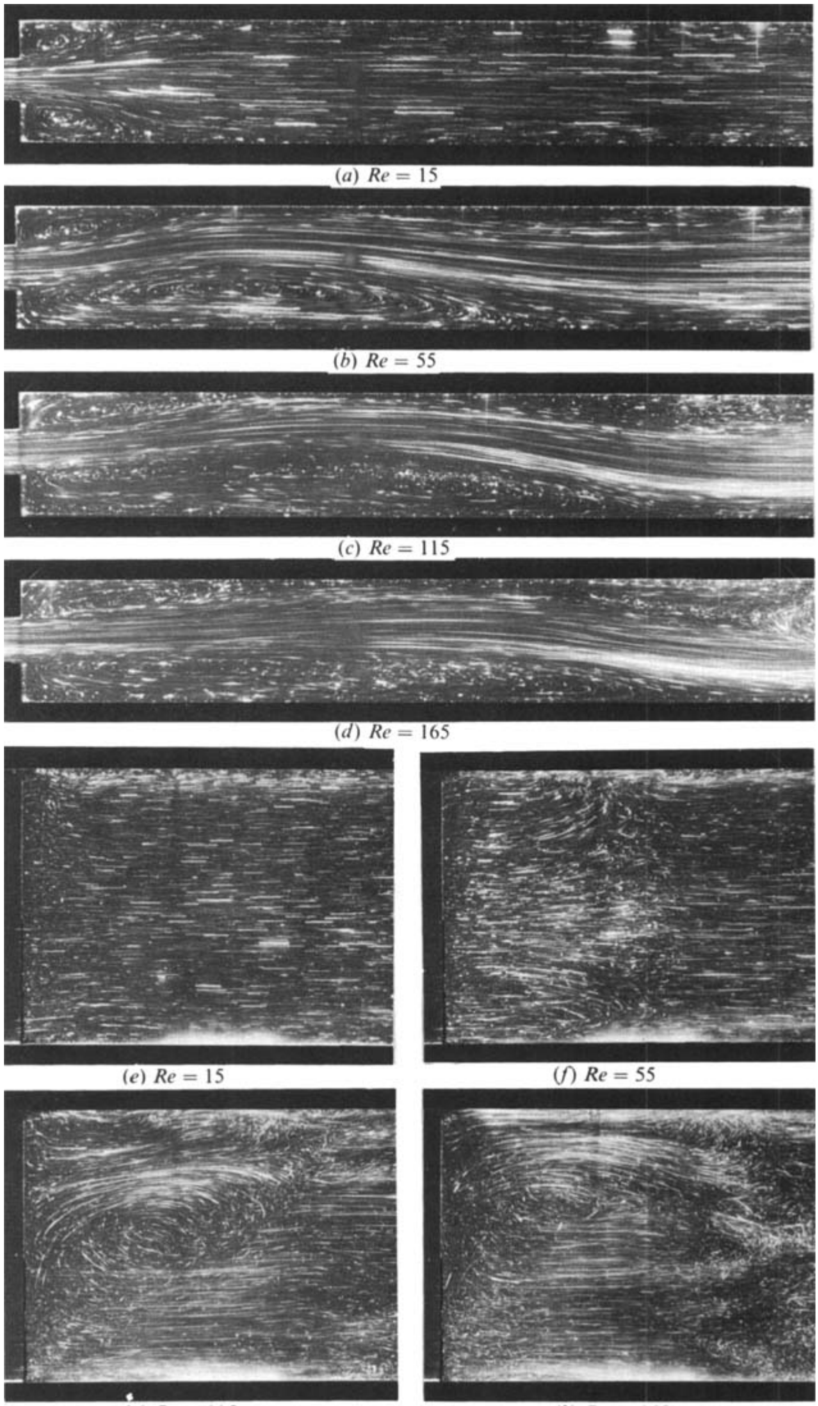

FIGURE 5. Steady flow through a symmetric expansion viewed from above and from the side; (a) $Re = 15$, (b) $Re = 55$, (c) $Re = 115$, (d) $Re = 165$, (e) $Re = 15$, (f) $Re = 55$, (g) $Re = 115$, (h) $Re = 165$.

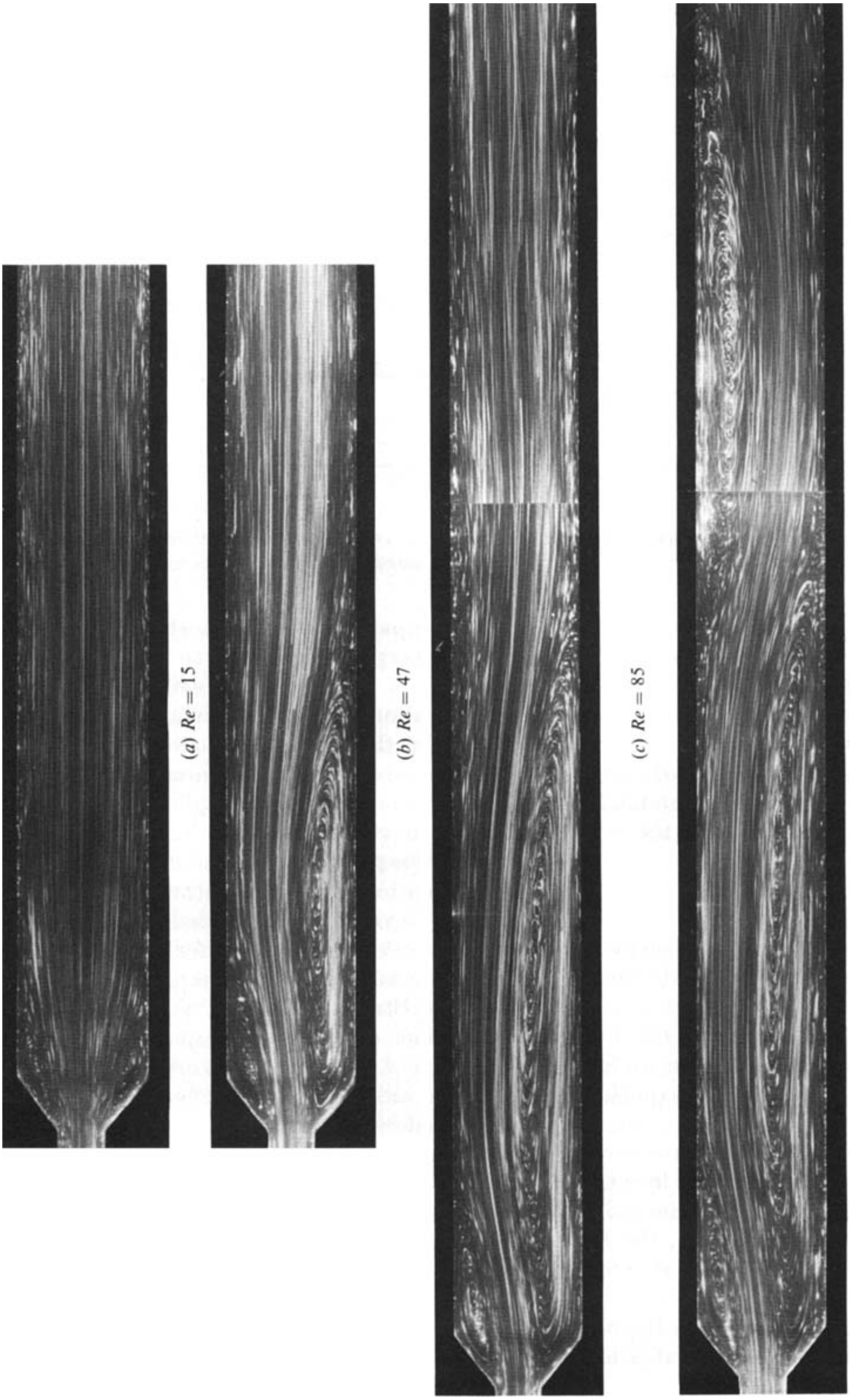

FIGURE 6. Steady flow through a symmetric 45° expansion. (a) $Re = 15$, (b) $Re = 47$, (c) $Re = 85$, (d) $Re = 115$.

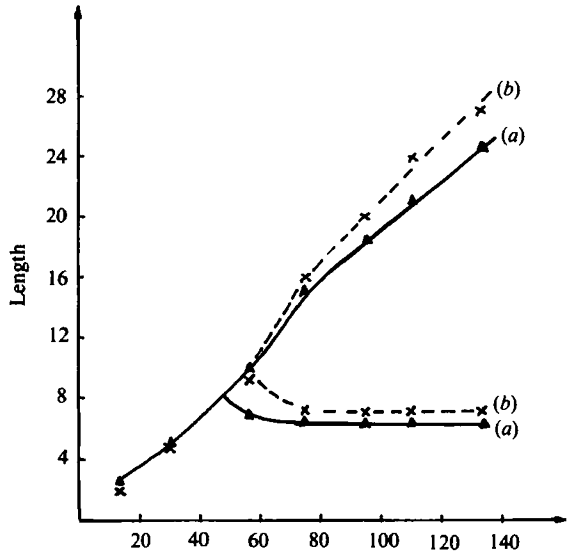

FIGURE 7. Variation of vortex length on upper and lower walls in a symmetric expansion as Reynolds number varies: (*a*) right-angled expansion, (*b*) 45° expansion.

this time that the secondary vortex began to expand into the mainstream. At that stage the mainstream had a noticeable wave superposed on it. As the flux continued to decrease, the wave was accentuated and a sequence of vortices appeared downstream (see figure 8*c*). Continued deceleration caused the vortices to expand, those downstream became more noticeable and at the instant of zero flux the channel was occupied by a wave of vortices. As the flux reversed, the fluid must have passed around the vortices, gradually entraining them into the mainflow until they disappeared. Note that the vortices did not move downstream, but as each one appeared on the wall it either remained in the same place or moved slightly upstream.

In order to study the vortex wave systematically we concentrated on taking photographs at one time in the cycle whilst the Reynolds and Strouhal numbers were varied. In figures 9–11 we show the development of the vortex wave for three Strouhal numbers and five Reynolds numbers. The general features are summarized first before we comment on interesting details. At a fixed Strouhal number, as the Reynolds number was increased the longitudinal extent of the wave rapidly increased. Corresponding to this was an increased strength of the individual vortices. Thus the damping of the wave was quickly decreased and indeed as shown in figure 11 the flow experienced a burst of turbulence during the deceleration. This occurred at what might be considered quite a small Reynolds number, $Re = 180$. We believe these photographs support the idea that at a critical value of the parameters the wave was neutrally damped and that led to the turbulent burst (see discussion below).

If, on the other hand, the Reynolds number is fixed and the Strouhal number decreased the longitudinal extent of the wave also increased. More importantly the wavelength increased noticeably, showing a strong dependence on the Strouhal number. A change in the Reynolds number did not have such a significant effect on the wavelength, but examination of the position of the third vortex in figure 10 shows a consistent downstream movement. To summarize, the wavelength appeared strongly dependent on St but only weakly dependent on Re.

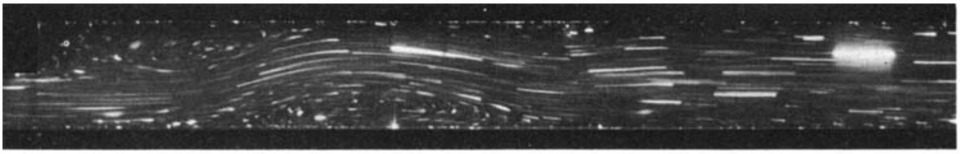

(*a*)

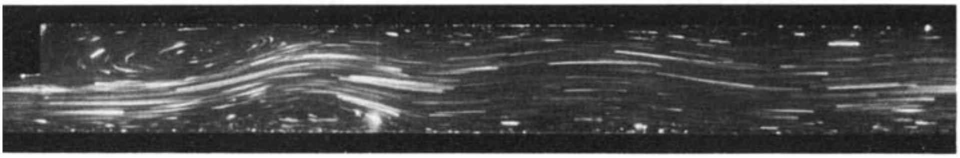

(*b*)

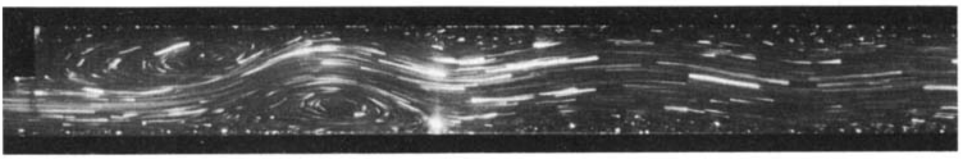

(*c*)

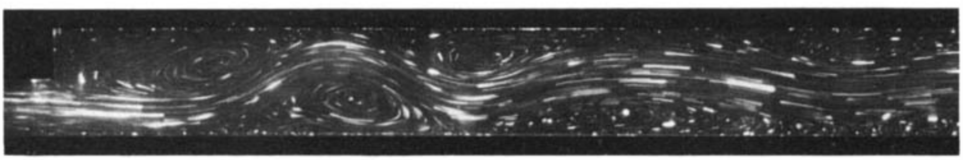

(*d*)

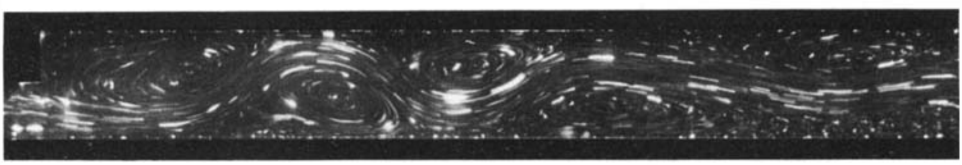

(*e*)

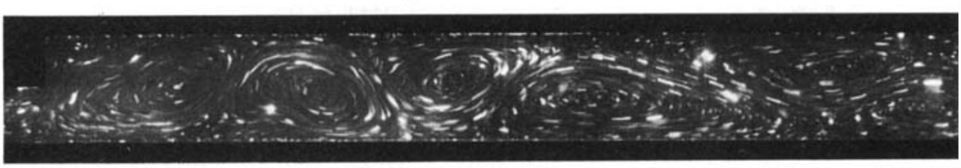

(*f*)

(*g*)

FIGURE 8. Observation of a vortex wave through a right-angled expansion ($Re = 80$, $St = 0.003$): (*a*) $t = 0.25$, (*b*) $t = 0.39$, (*c*) $t = 0.42$, (*d*) $t = 0.44$, (*e*) $t = 0.47$, (*f*) $t = 0.5$, (*g*) $t = 0.53$.

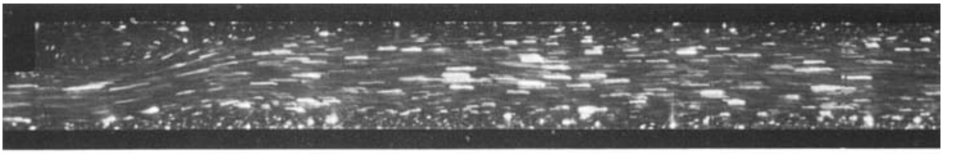

(a)

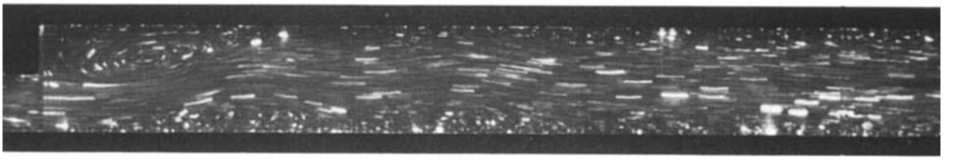

(b)

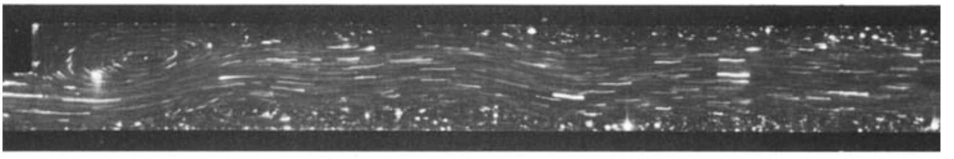

(c)

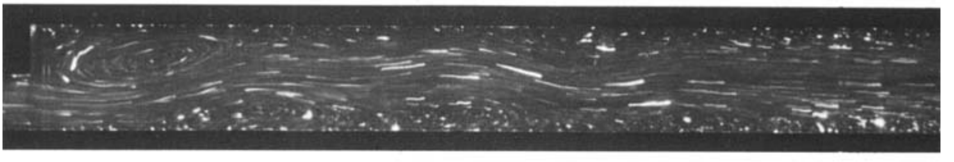

(d)

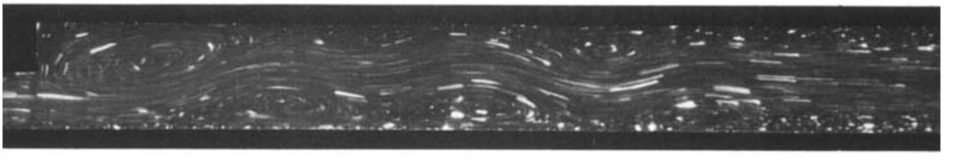

(e)

FIGURE 9. Flow at a fixed time of $t = 0.42$ and $St = 0.004$ as the Reynolds number varies: (a) $Re = 45$, (b) $Re = 60$, (c) $Re = 75$, (d) $Re = 90$, (e) $Re = 105$.

There are some details worthy of specific note. In figure 9(d) there is a connected double vortex. The secondary vortex has split into two and that appeared to inhibit separation on the upper wall where only a small vortex has formed. Further downstream on the upper wall a larger (and presumably stronger) vortex formed. This demonstrated the delicate bifurcation phenomenon which can exist in separated flows and also that the observed amplitude of the vortex wave need not decrease monotonically with distance along the channel. Vortex splitting can also be seen in figure 11(c) in the third vortex on the upper wall. The shape of the vortices appears to be closer to elliptical than circular and during the deceleration the semi-major axis rotated until it was at a considerable angle to the mainflow direction. This can be seen for example in figure 11, third and fourth vortices. The rotation of the vortices makes possible further separation on the wall and under the existing vortex. Note that in vortex splitting two co-rotating vortices form whilst separation at the rear of an existing vortex would produce a counter-rotating vortex.

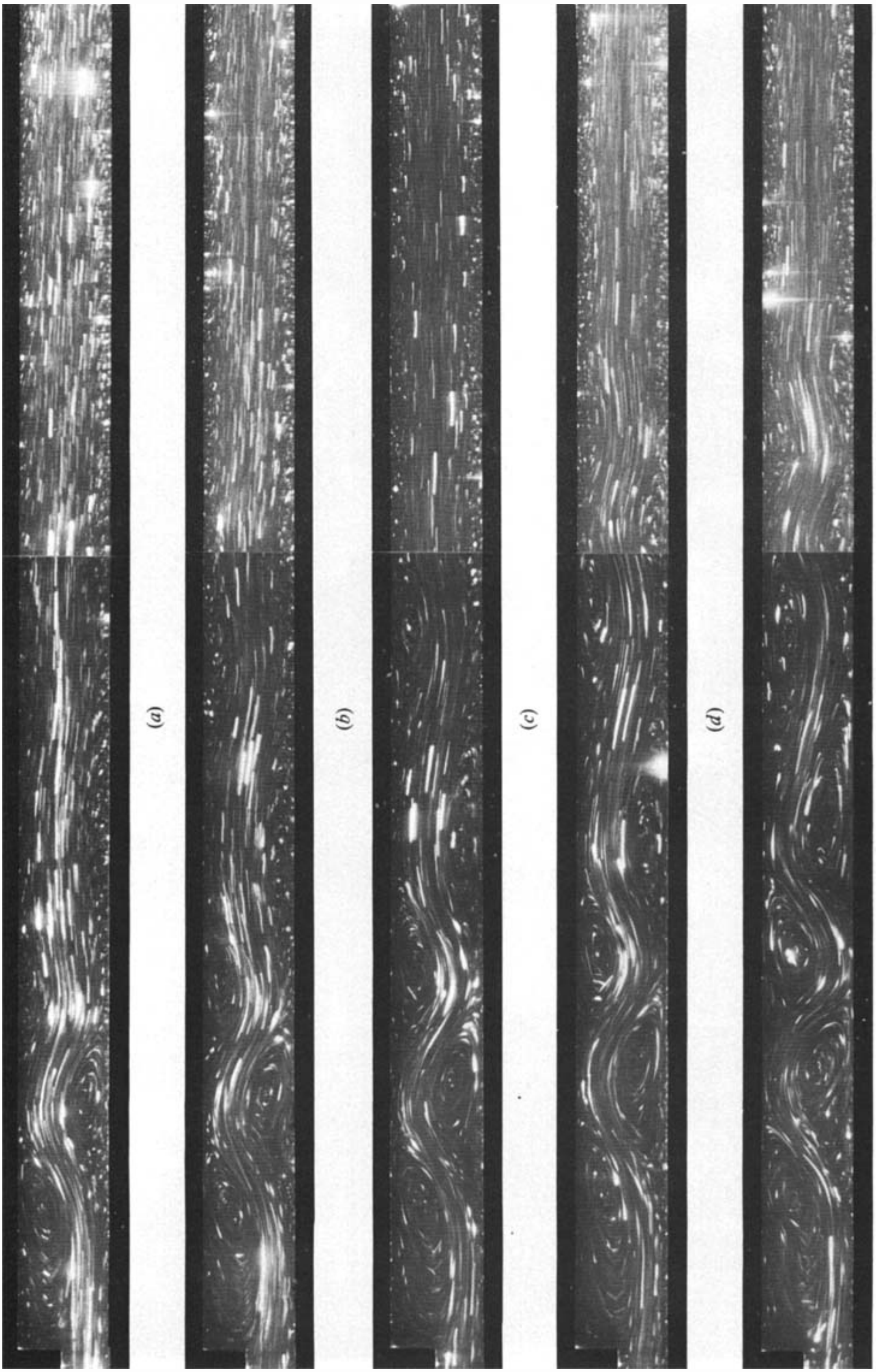

FIGURE 10. Flow at a fixed time of $t = 0.42$ and $St = 0.003$ as the Reynolds number varies: (*a*) $Re = 60$, (*b*) $Re = 80$, (*c*) $Re = 100$, (*d*) $Re = 120$, (*e*) $Re = 140$.

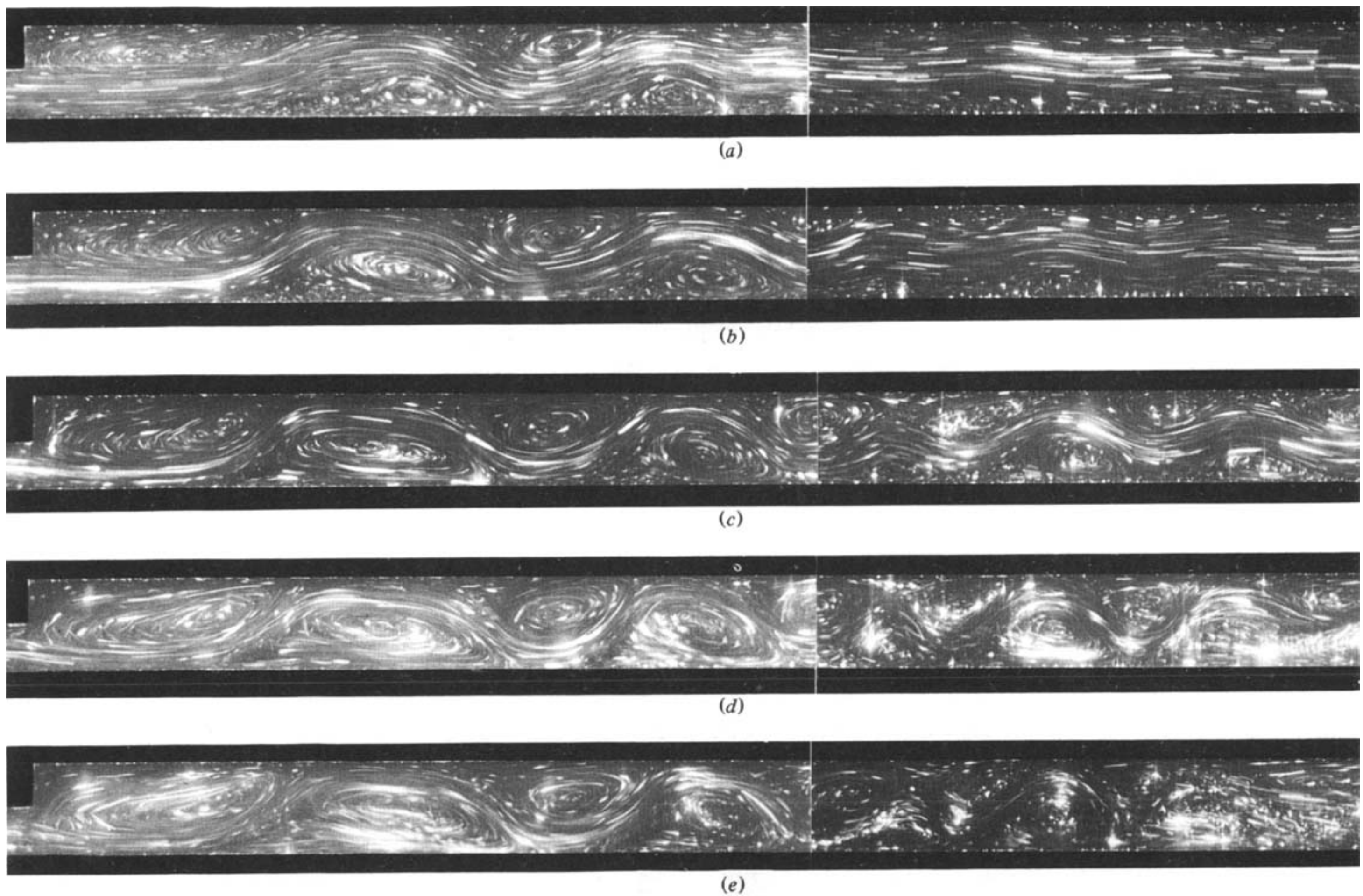

FIGURE 11. Flow at a fixed time of $t = 0.42$ and $St = 0.002$ as the Reynolds number varies: (a) $Re = 90$, (b) $Re = 120$, (c) $Re = 150$, (d) $Re = 180$, (e) $Re = 210$.

We have observed the flow from the side of the channel so as to examine any three-dimensional effects which may have been present. In figure 12 we show photographs at two Strouhal numbers and two Reynolds numbers each at peak flow and during the deceleration. In each case a three-dimensional corner vortex was present and increased in size when the Reynolds number increased or the Strouhal number decreased. The photographs were taken by illuminating the upper half of the channel (i.e. behind the step) and they show the primary vortex followed by a band of high shear on the wall opposite the secondary vortex. It is clear that the flow near the centre of the channel was two-dimensional at peak flow for a wide range of *Re* and *St* (figure 12(*a*, *c*, *e*, *f*)). During the deceleration that was not true and at high *Re* a turbulent burst appeared, as can be seen from the striations of figure 12(*g*) in the third vortex. Note that flow in the primary vortex near the centre of the channel still appeared to be two-dimensional and laminar.

If, instead of a right-angled expansion, a 45° expansion occurred then the global details changed little. This can be illustrated by the vortex wave during the deceleration for two Strouhal numbers in that geometry (figures 13 and 14). In figure 13, when the Strouhal number was $St = 0.003$, the lateral extent of the wave grew rapidly with increased Reynolds number and again vortex splitting was apparent (figure 13(*d*)). In figure 14, when $St = 0.002$, a turbulent burst again is produced, but now the Reynolds number for that event has decreased compared to that for the same event during flow through a right-angled expansion. This was contrary to our expectations since we would have thought that the sudden expansion would have promoted turbulence at a lower Reynolds number than the relatively slow 45° expansion. We can offer no explanation of this observation but note that the same is found in a symmetric expansion (see §4.2 below).

4.2. *Symmetric channels*

We have observed oscillatory flow in a symmetric channel and an asymmetric flow occurred during the deceleration. In figure 15 we show the flow during one cycle. At the beginning of the cycle there was some residual motion from the previous half-stroke. That appeared to have the form of two slowly moving layers, one adjacent to each wall. At peak flow (figure 15*b*) a vortex had formed on each wall and the vortices appeared to be symmetric. Further downstream, though, an asymmetric flow had been established with the generation of a small vortex on each wall and the appearance of a wave in the mainflow. During the deceleration the wave grew and the primary vortices became asymmetric. More vortices appeared further downstream. Continued deceleration increased the size of the vortices and the longitudinal extent of the wave. A new phenomenon had appeared and that was the movement of the vortices downstream (see figure 15(*c*, *d*), primary vortex on the upper wall). In the asymmetric channels there appeared to be no movement of the vortices downstream after they had formed: indeed there was a tendency for them to move upstream. Further splitting of the vortices occurred as can be seen in figure 15(*d*, *e*), in the primary vortices.

If the Strouhal number was fixed and the Reynolds number increased the result was not identical with that observed in the asymmetric channel. At first, the longitudinal penetration of the vortex wave seems greater in the symmetric channel, as can be seen by comparing figure 16 with figure 10. The vortices appear stronger and the turbulent burst during the deceleration occurred at a lower Reynolds number and a higher Strouhal number than in the comparable asymmetric expansion. Examination of figure 16(*b*–*e*) shows that the wave did not attain the longitudinal

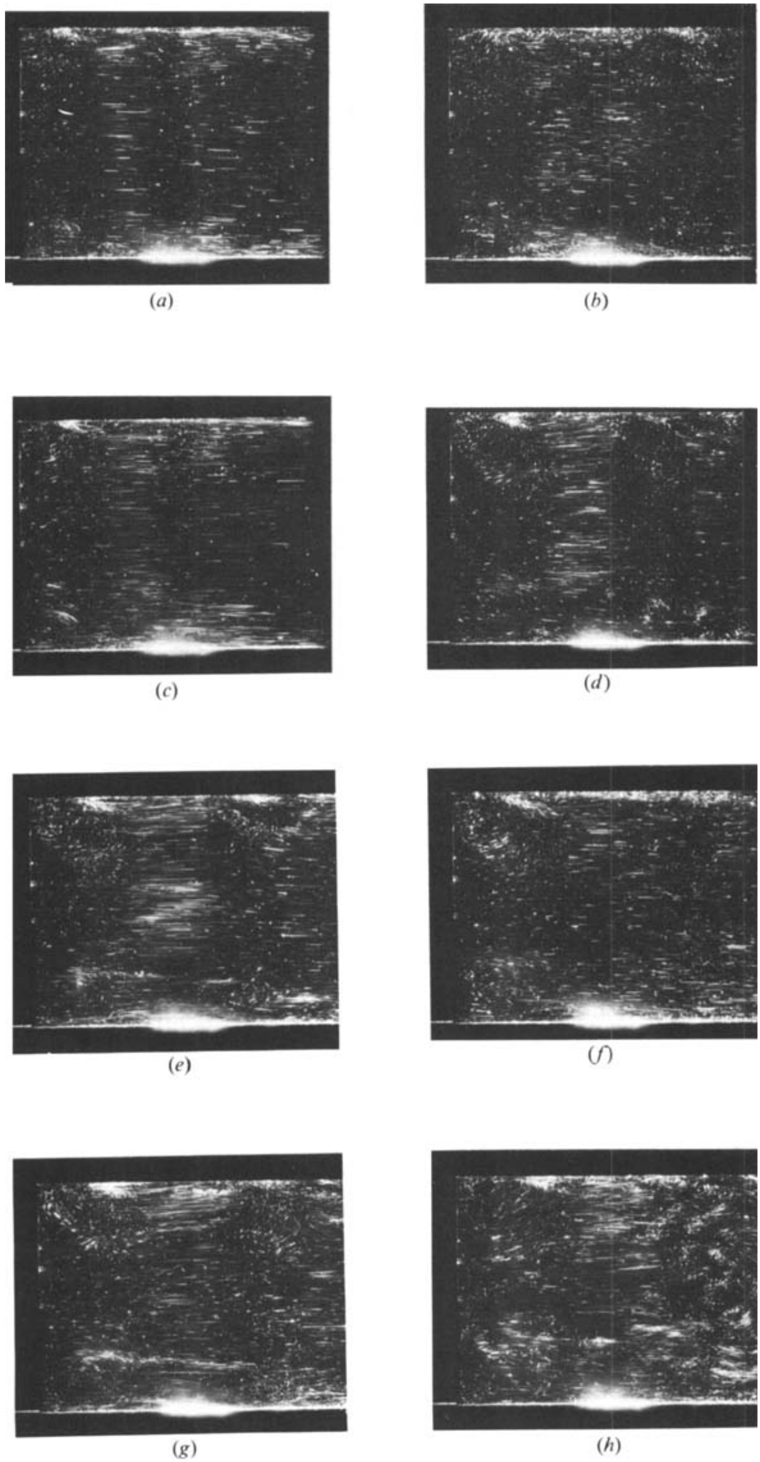

FIGURE 12. Observation of flow from the side of channel: $Re = 80$, $St = 0.003$ (a) $t = 0.25$, (b) $t = 0.42$; $Re = 120$, $St = 0.003$, (c) $t = 0.25$, (d) $t = 0.42$; $Re = 120$, $St = 0.002$; (e) $t = 0.25$; (f) 0.42; $Re = 150$, $St = 0.002$; (g) $t = 0.25$, (h) $t = 0.42$.

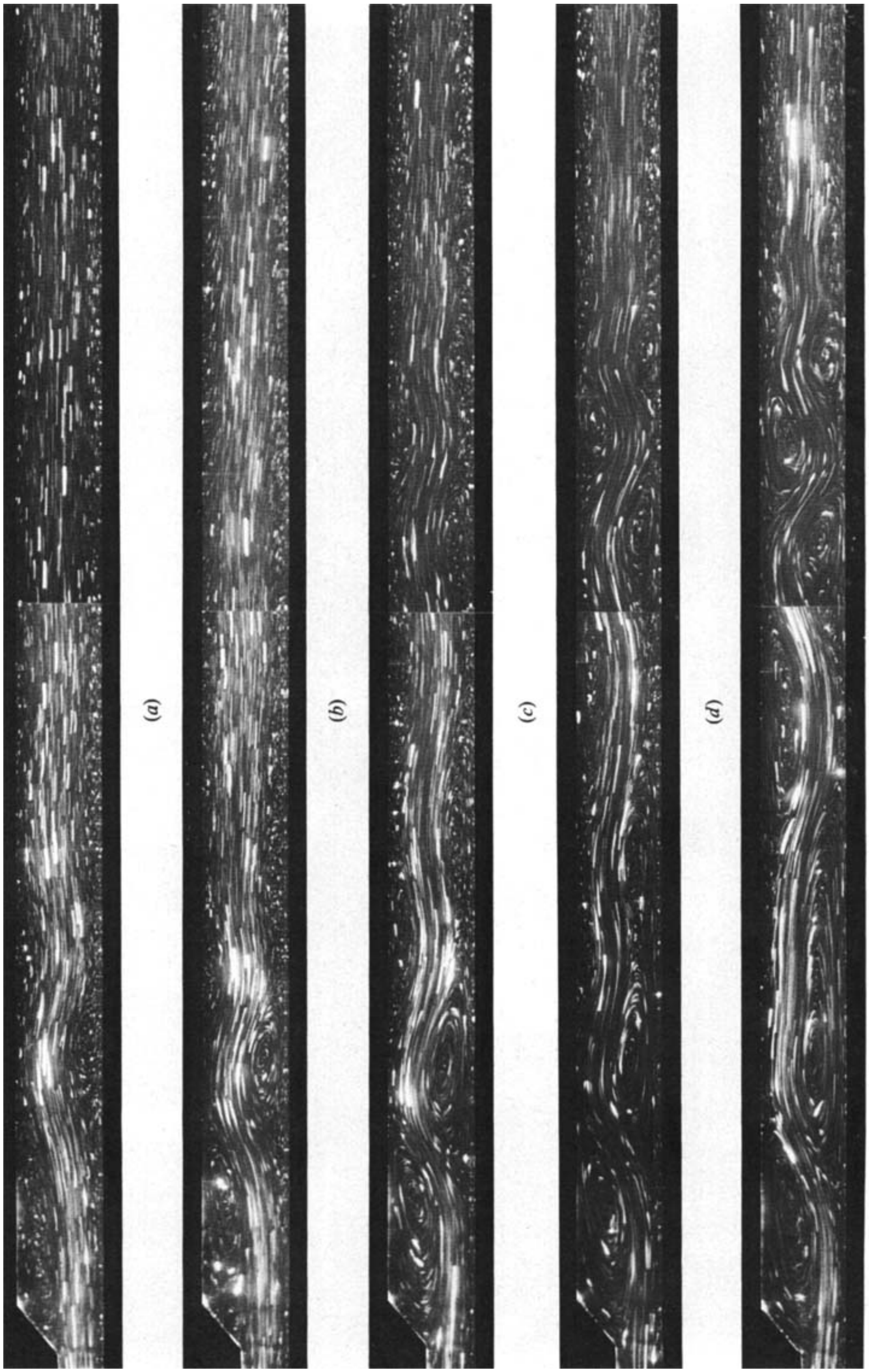

FIGURE 13. Flow through a 45° expansion at a fixed time $t = 0.42$ and $St = 0.003$ as the Reynolds number varies: (a) $Re = 60$. (b) $Re = 80$. (c) $Re = 100$, (d) $Re = 120$, (e) $Re = 140$.

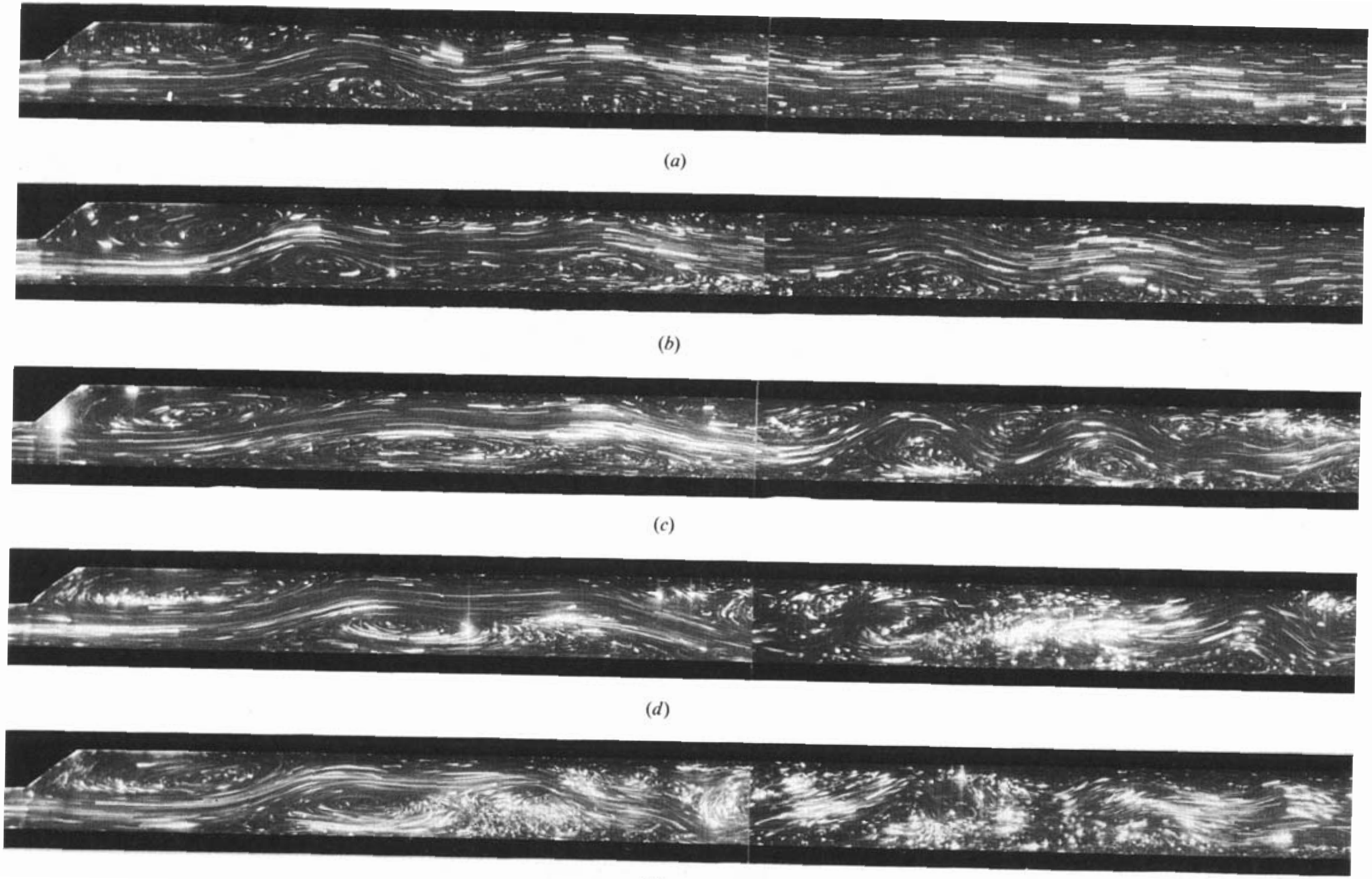

FIGURE 14. Flow through a 45° expansion at a fixed time $t = 0.42$ and $St = 0.002$ as the Reynolds number varies: (a) $Re = 90$, (b) $Re = 120$, (c) $Re = 150$, (d) $Re = 180$, (e) $Re = 210$.

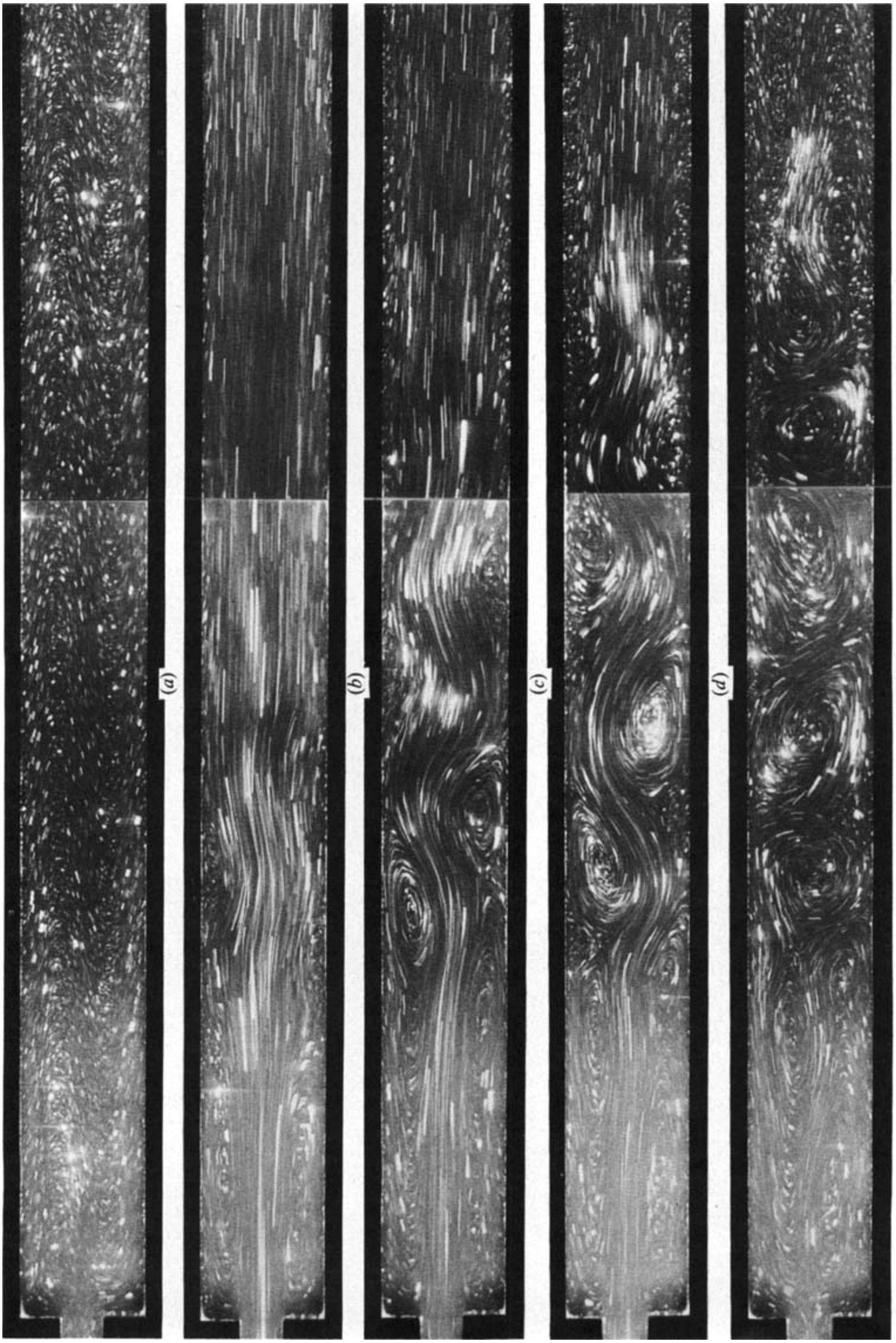

FIGURE 15. Oscillatory flow through a symmetric channel, $Re = 80$, $St = 0.003$: (*a*) $t = 0$; (*b*) $t = 0.25$, (*c*) $t = 0.33$, (*d*) $t = 0.42$, (*e*) $t = 0.5$.

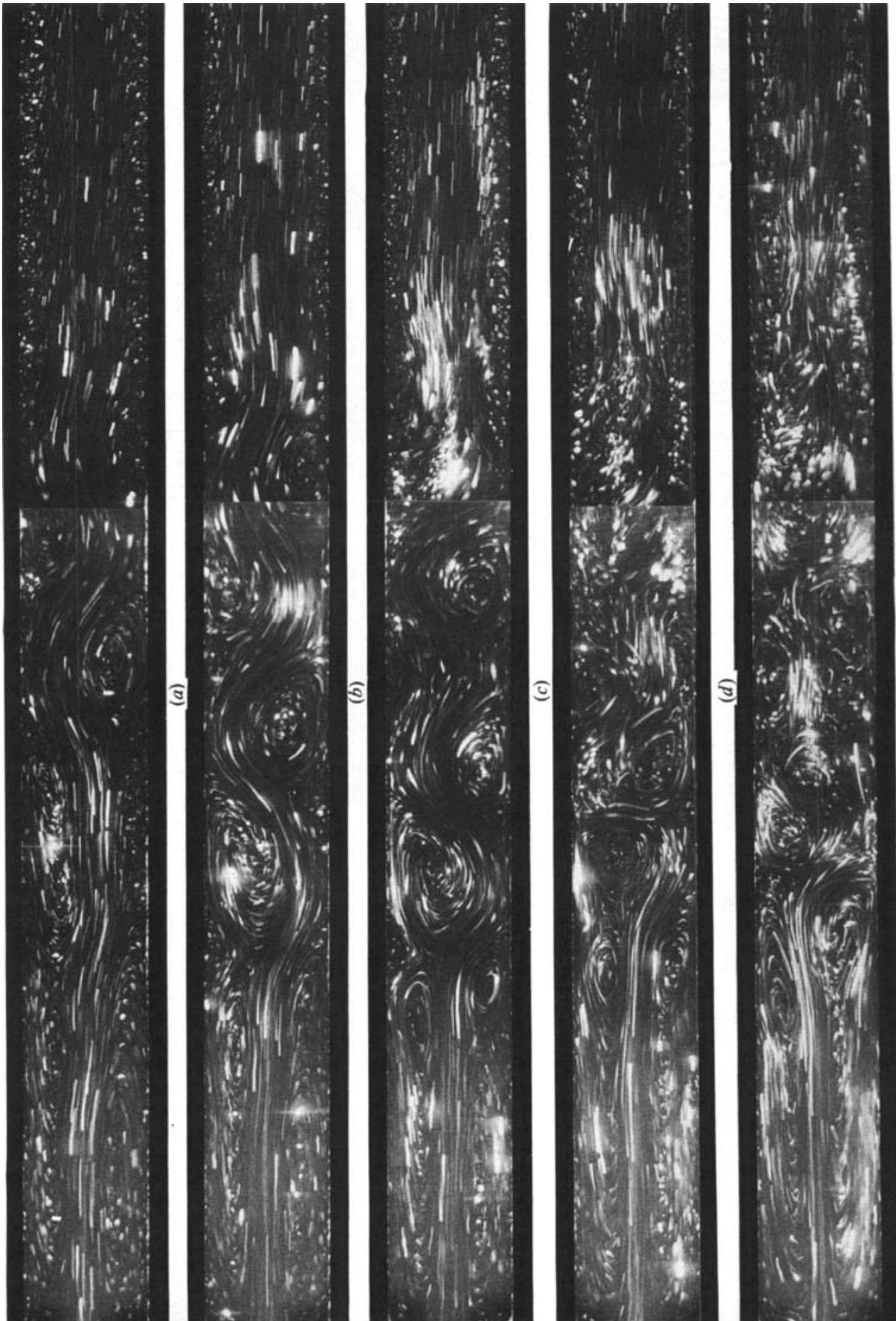

FIGURE 16. Flow through a right-angled symmetric expansion at a fixed time $t = 0.42$ and $St = 0.003$; (a) $Re = 60$, (b) $Re = 80$, (c) $Re = 100$, (d) $Re = 120$, (e) $Re = 140$.

extent of that in an asymmetric channel, and the increasing intensity of the turbulent burst occurred with decreased longitudinal extent of the wave. Recalling that it was the fluid flux that was decreasing, this observation suggests that the vortex wave observed in a symmetric channel is a dissipative process enabling the fluid to eliminate excess kinetic energy as the flux decreases.

If a symmetric 45° expansion is used (figure 17), again a wave was observed, but now the turbulent burst occurred at an even lower Reynolds number than in the right-angled symmetric expansion. In this channel there was also a contraction of the longitudinal extent of the turbulent burst as the Reynolds number increased.

5. Calculated flow patterns

We have calculated the oscillatory flow in a two-dimensional channel by solving the unsteady Navier–Stokes equations using a finite-difference scheme. A description of our method of solution has been given elsewhere (Sobey 1980, 1982) and we only repeat a few details here. We assumed that we were dealing with flow in a longitudinally periodic channel, in this case one whose periodic length was much greater than the lateral width of the channel. The assumption of spatial periodicity allows the boundary conditions applied to be exact since the solution can be iterated until the upstream and downstream values of the stream function match. This device eliminated the need to use approximate upstream conditions and the solution did not have to be stopped when reversed flow occurred near the downstream boundary. The stream function and vorticity form of the equations were put into finite-difference form by using upwind differencing and a Dufort–Frankel two time-level substitution. A fine mesh was used near the boundaries and a coarser one near the centre of the channel. Altogether some 7100 mesh points were distributed through the computational region and a time step of 0.001 to 0.0005 was typical.

The solution was calculated for periodic flux through the channel ($q = 2\sin 2\pi t$) and the flow started from rest. In the first time step the flow was potential except at the walls, where thin layers of vorticity were represented by non-zero wall vorticity, but zero vorticity in the interior of the channel. Our past experience has been that when the flow is dominated by viscosity (i.e. *Re* very small or *St* large) the perturbation caused by the starting condition is then considerable and the calculation of several cycles is necessary to obtain a time-periodic solution. When the flow is dominated by inertial effects the initial perturbation generally became negligible during the initial acceleration so that the second half-cycle exemplified the time-periodic solution and the deceleration period in the first half-cycle was a reasonable representation of the flow during subsequent periods of deceleration. The rapid decay of starting transients is consistent with our experimental observations.

The numerical results we present support the experimental observations but do not form a comprehensive study of the flows we have observed. We hope to produce such a study at a later date. The calculations are for a sinusoidal expansion at one end and a similar contraction at the other end. Thus if (x, y) are cartesian coordinates non-dimensionalized by half the minimum channel gap (see Sobey 1982) the boundaries of the channel were described by

$$y = \begin{cases} 1 + \frac{1}{2}(D-2)\left\{1 - \cos\dfrac{2\pi x}{L_1}\right\}, & 0 < x < L_1,\ L - L_1 < x < L, \\ D-1, \quad L_1 < x < L - L_1, & \end{cases}$$

and $\qquad y = -1$

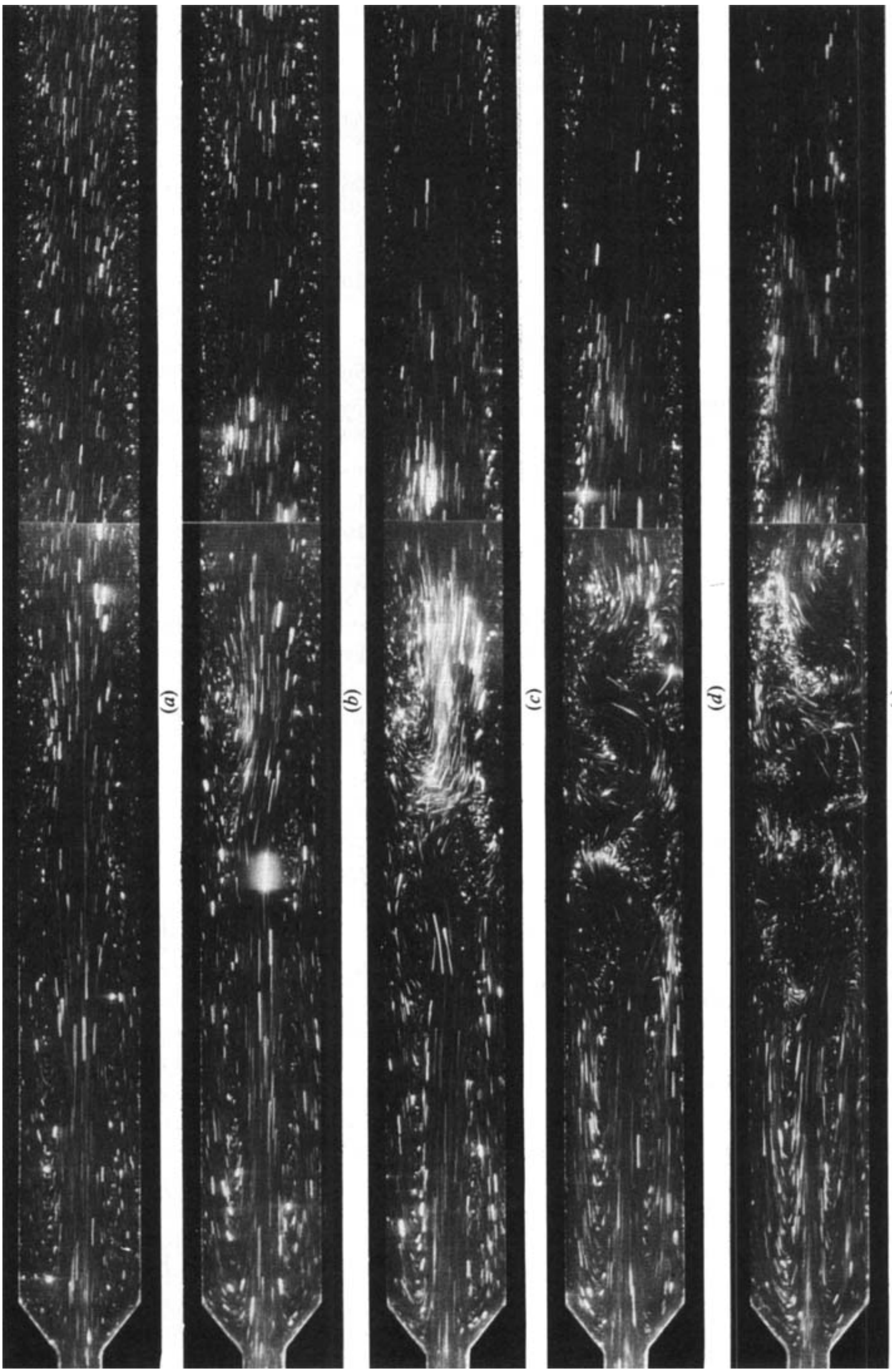

FIGURE 17. Flow through a 45° symmetric expansion at a fixed time $t = 0.42$ and $St = 0.003$; (a) $Re = 60$, (b) $Re = 80$, (c) $Re = 100$, (d) $Re = 120$, (e) $Re = 140$.

for an asymmetric channel, and for a symmetric channel both walls had a similar displacement. The numerical values used were $L = 40$, $L_1 = 4$ and $D = 4$. The calculations were performed on Bristol University's 'Multics' system and a single half-cycle required approximately six hours c.p.u. time. It was apparent from the calculations that the contraction at the end of the channel section could strongly influence the flow development and we hope that subsequent numerical studies will be able to deal with very much larger values of the channel length L and also steady flow.

5.1. *Asymmetric channels*

We show in figure 18 the streamlines calculated during the initial half-cycle when $Re = 125$ and $St = 0.01$. It can be seen that at peak flow a vortex exists on both walls. The flow cannot then be quasi-steady since our steady-flow observations did not show a vortex on the lower wall. As the flow decelerates (figure 18*b*) the size of the vortices increases and the reattachment point moves downstream. Then a separate detached region appears on the upper wall (figure 18*c*) and a third vortex forms. Another notable feature is the rapid downstream movement of the point of reversal of wall shear. This occurs on both the upper and lower walls and the flow downstream of the vortices is parallel, but with a thin reverse-flow layer at each wall. At $t = 0.45$ (figure 18*d*) a noticeable wave has appeared as the core flow passes between the growing vortices. This process continues until at the instant of zero flux (figure 18*e*) there remain only the vortices with a wavy dividing streamline between them. Reversal of the flux forces the fluid to move around the existing vortices (figure 18*f*). These patterns should be compared with figure 8 where the same principal features were observed.

If the Strouhal number is fixed and the Reynolds number increased then the wavelike nature of the flow patterns becomes more pronounced. In figure 19 we show calculations for $St = 0.005$ at a fixed time $t = 0.45$, and for Reynolds numbers between 75 and 150. It can be seen that there appears to be little change in the size of the vortices, in agreement with the observed flow patterns. In figure 19(*d*) the vortex on the lower wall appears to be displaced upstream and there is a suggestion that vortex splitting has occurred on the upper wall. Note also that the calculations are at $t = 0.45$ whilst the observations were nominally at $t = 0.43$. This is because the time of exposure of the film during the experiments was $\frac{1}{60}$ s and so the observations are actually an 'integrated' view during $t = 0.43$ to $t = 0.46$, the exact length of time depending on the piston frequency.

If the Reynolds number is fixed at $Re = 125$ and the Strouhal number decreased, the calculations again show close agreement with the qualitative features of the observations. In figure 20 the size of the vortices increases markedly with decreasing Strouhal number. This is to be expected since decreasing Strouhal number corresponds to increasing particle displacement and that should produce longer and stronger vortices.

5.2. *Symmetric channels*

When solving the Navier–Stokes equations, either numerically or analytically, the existence of symmetry can be used to reduce the size of the problem. In numerical solutions the area is smaller and, in the case of a symmetric channel, only one half the area need be considered. The symmetry is imposed by insisting that the channel centreline is a streamline. This will preclude the calculation of asymmetric flows regardless of whether such flows are stable or unstable. When the full channel is considered, although the boundary conditions may be symmetric, the calculation of

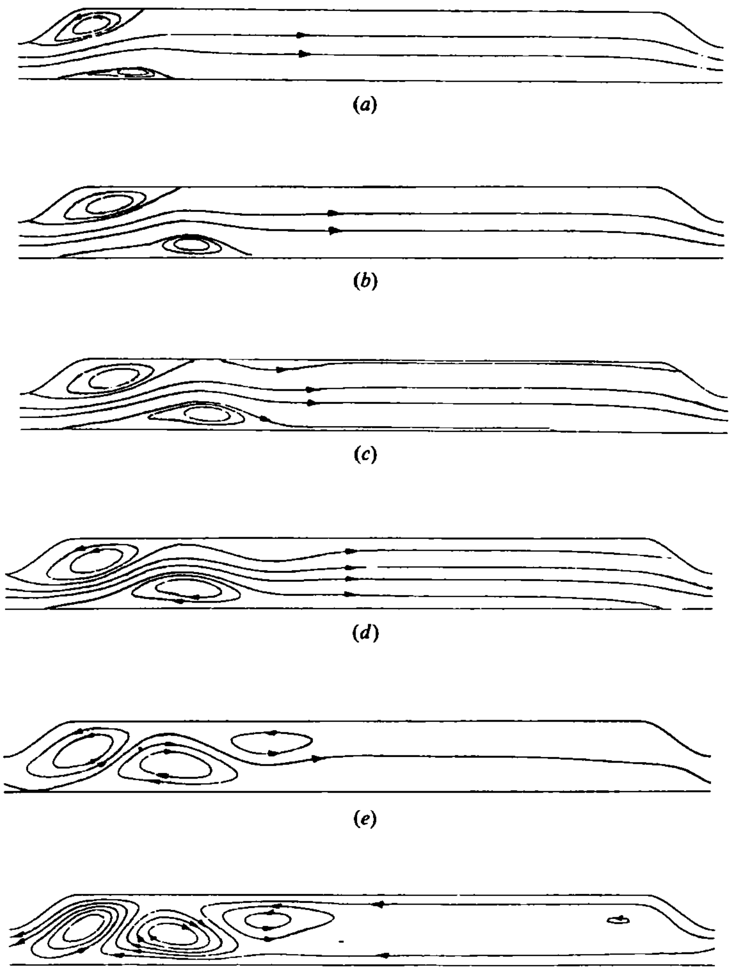

(f)

FIGURE 18. Calculated streamlines through an asymmetric channel, $Re = 125$, $St = 0.01$: (a) $t = 0.25$, (b) $t = 0.35$, (c) $t = 0.40$, (d) $t = 0.45$, (e) $t = 0.5$, (f) $t = 0.52$.

asymmetric flows is possible. In order to confirm that our calculations are of an asymmetric flow and not the result of numerical instabilities in the method of solution we have performed one calculation with double the number of mesh points. An asymmetric flow was obtained but with the asymmetry in the opposite direction. This result shows that the flows we have calculated are indeed true solutions of the Navier–Stokes equations and not the result of fine details in our method of solution. Note that where two stable asymmetric solutions and one unstable symmetric solution exist the particular asymmetric solution which the numerical scheme calculates depends on the domain of attraction of each of the stable solutions. Since all numbers have finite representation on a computer the initial conditions used numerically will place the initial solution in the domain of attraction of one solution in a manner which cannot be predicted in advance and which may alter as the fine details of the numerical scheme are varied.

In figure 21 we show the flow patterns in a symmetric channel for $Re = 125$ and

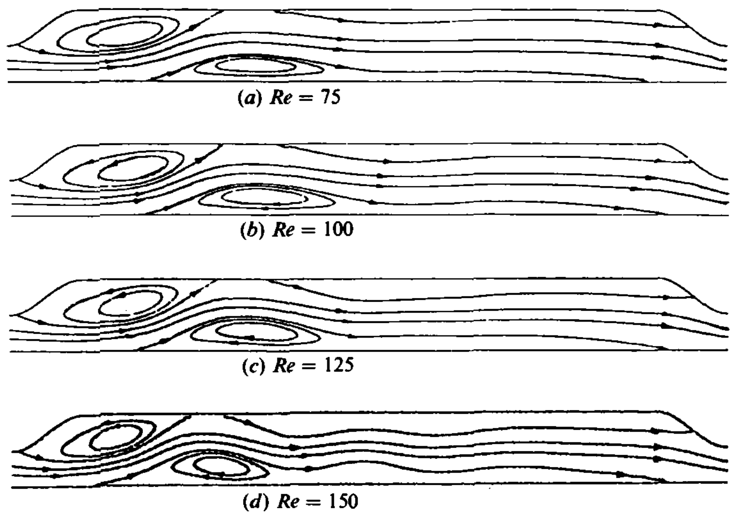

FIGURE 19. Calculated streamlines at a fixed time $t = 0.45$ and $St = 0.005$. (*a*) $Re = 75$, (*b*) $Re = 100$, (*c*) $Re = 125$, (*d*) $Re = 15$.

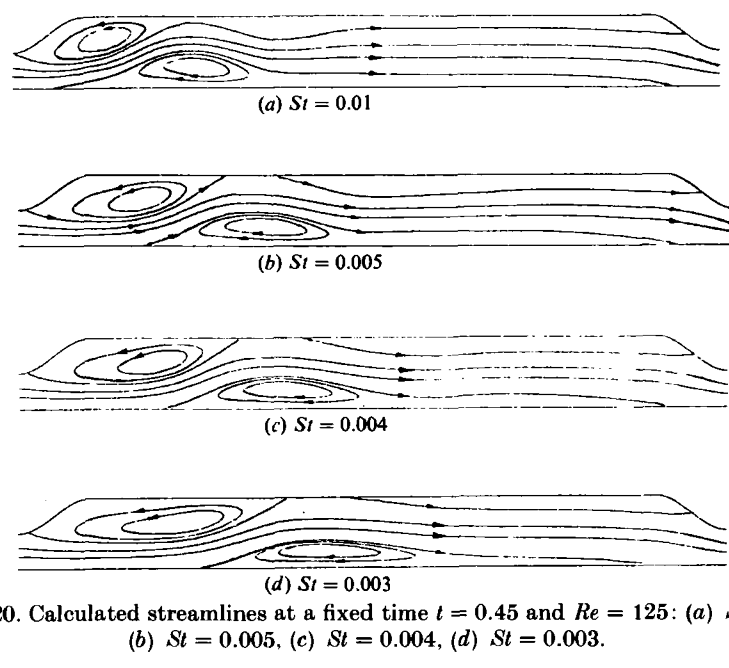

FIGURE 20. Calculated streamlines at a fixed time $t = 0.45$ and $Re = 125$: (*a*) $St = 0.01$, (*b*) $St = 0.005$, (*c*) $St = 0.004$, (*d*) $St = 0.003$.

$St = 0.01$. In this case the flow remains symmetric throughout the cycle. A pair of vortices form early in the acceleration and grow in longitudinal extent during the rest of the acceleration and the deceleration. We have measured the longitudinal extent of the vortices and that length is a linear function of the time integral of the flux (i.e. the distance that a fluid particle would have been displaced if there were a uniform velocity across the channel). This demonstrates that once the vortices are formed they are convected with a velocity which is somewhat less than the mean flow. This agrees with our observations and is a significant difference between flow in a

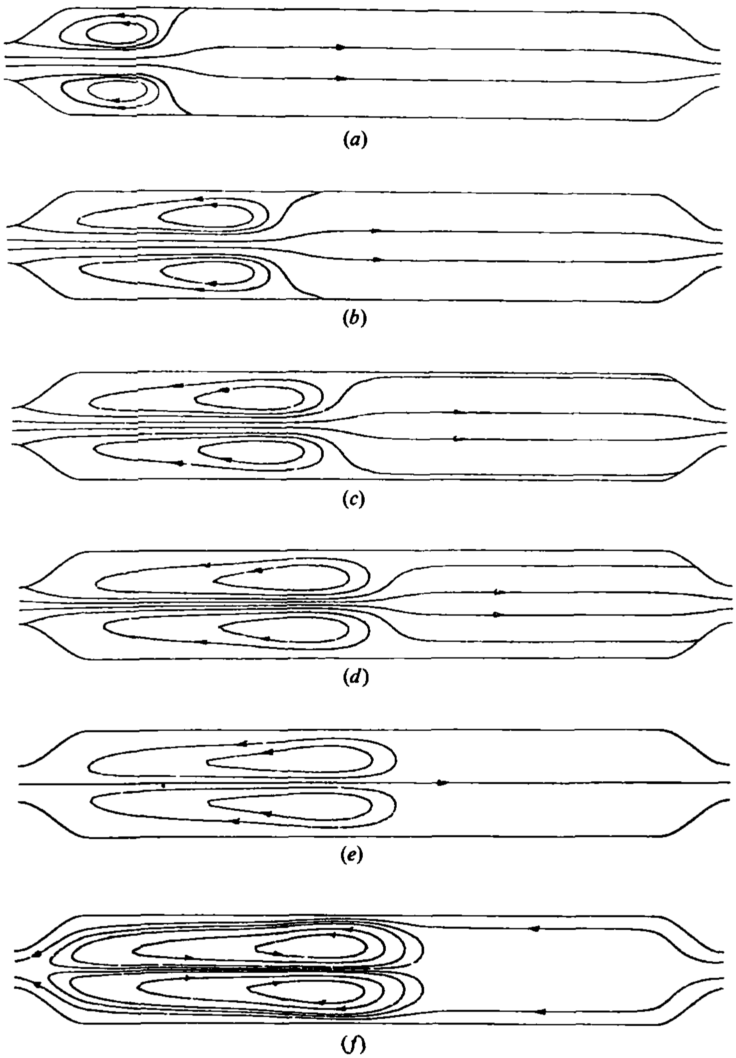

FIGURE 21. Calculated streamlines in a symmetric channel, $Re = 125$, $St = 0.01$: (a) $t = 0.25$, (b) $t = 0.35$, (c) $t = 0.40$, (d) $t = 0.45$, (e) $t = 0.5$, (f) $t = 0.52$.

symmetric channel and flow in an asymmetric channel, where individual vortices are not convected by the flow once they have formed.

If the Strouhal number is lowered to $St = 0.005$ the flow remains symmetric during the initial part of the acceleration. As the vortices are convected downstream an asymmetric disturbance appears and as the vortex on the upper wall bulges in the centre, the vortex on the lower wall bulges at each end. This is shown in figure 22 (c). Continued deceleration accentuates this effect and the vortices on each wall split, with a wave appearing in the core of the channel. When the flux vanishes we have a system of vortices alternating on each wall with a wavy dividing streamline. These calculations should be compared with figure 15. It is apparent that the formation of a wave in the symmetric channel is not attributable to the mechanism which produced the vortex wave. In an asymmetric channel the vortex wave results from a coupling of the lateral pressure gradient to the longitudinal velocity shear (see I).

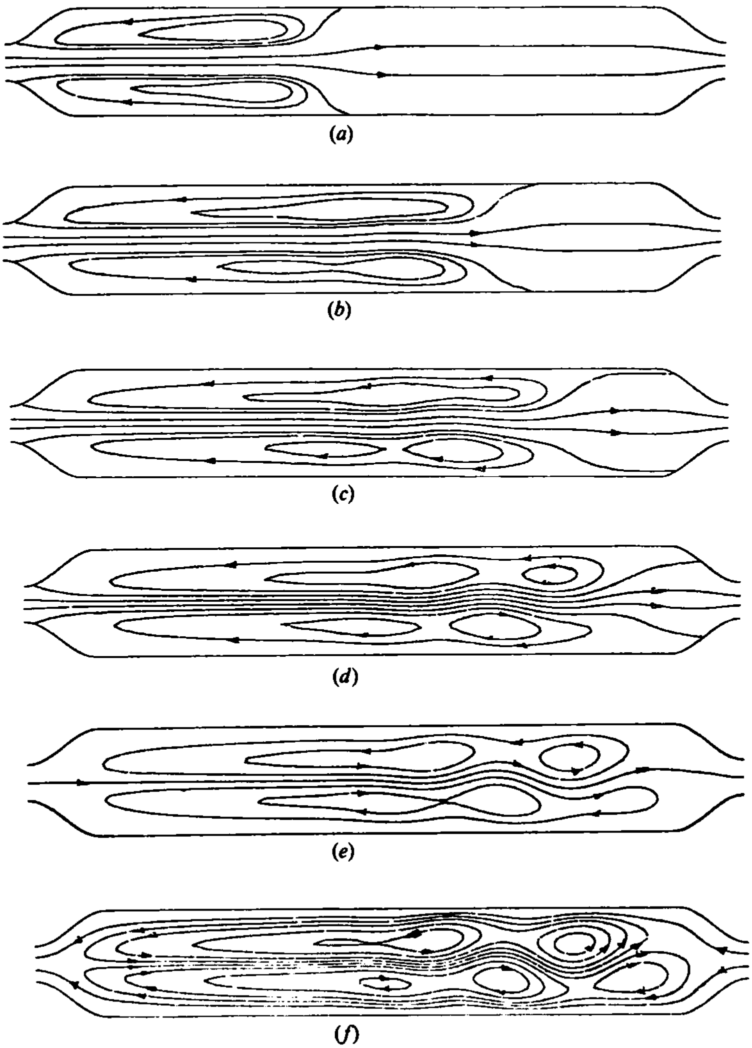

FIGURE 22. Calculated streamlines in a symmetric channel, $Re = 125$, $St = 0.004$: (*a*) $t = 0.25$, (*b*) $t = 0.35$, (*c*) $t = 0.40$, (*d*) $t = 0.45$, (*e*) $t = 0.5$, (*f*) $t = 0.52$.

In the symmetric channel the wave appears to be the result of an instability during the deceleration of the shear layer between the two vortices as they are convected downstream. The wave is the result of the two initial vortices being split into parts. In the asymmetric channel the vortex wave is not produced by the splitting of vortices, although the vortices which make up the vortex wave may themselves split. Clearly there is much we do not yet understand about this matter.

6. Discussion

6.1. *Steady flow*

Our observations of steady flows agree extremely well with the literature. In an asymmetric channel the linear increase in vortex length is well known. In the case of a symmetric channel previous observations by Cherdron *et al.* (1978) and Durst *et al.* (1974) have shown the existence of asymmetric flow and also that the asymmetries are observed at the lowest Reynolds number when the expansion ratio is 1 : 3. The limiting length of the smaller vortex appears to be a new observation and our observation from the side of the channel sheds some new light on the breakdown from two- to three-dimensional motion. The value of the Reynolds number at which asymmetries appear is in close agreement with their observations. Most recently John (1984) has studied the stability of the symmetric flow. The basic problem of determining when non-unique solutions to the Navier–Stokes equations occur remains unresolved. Smith (1976*a*, *b*) has shown how the symmetric state can be described asymptotically. In Smith (1977) the flow far upstream of a disturbance (in that case asymmetric) was considered as an eigenfunction problem in a parallel channel. He showed that an eigensolution could be found in the upstream region but, as the disturbance was approached, a singularity in the solution developed and he did not attempt to carry the numerical solution past the point of the singularity, although some properties of the singularity were investigated. In a symmetric channel, one way for an asymmetry to arise is via an eigensolution as in Smith (1977). Such a solution would seem to have the correct properties since, as observed by Smith (1977), if one wall layer thickens it will cause a thinning of the other wall layer. Thus a small asymmetric disturbance might be able to grow from the free interaction of the lateral pressure gradient and the longitudinal velocity perturbation.

6.2. *Unsteady flow: asymmetric channels*

Our observations of vortex waves raises the question of how such waves can be generated. Firstly, it is worth asking if there is any wavelike structure in the solution for steady flow through an asymmetric channel. The asymptotic analysis of such flows has been given by Smith (1976*a*, *b*). If the channel extends from $y = \epsilon^2 HF(\epsilon x)$ to $y = 2$ and a longitudinal coordinate $X = \epsilon x$ is used, the solution for the core where $y = O(1)$, is

$$u \sim U_0(y) + \epsilon^2 A(x)\, U_0'(y), \quad v \sim -\epsilon^3 A'(x)\, U_0(y),$$

where $U_0(y) = \frac{3}{4}y(1-y)$ is the unperturbed flow and $A(X)$ is an unknown displacement function. The equations of motion show that the correct scaling for the case in which the viscous boundary-layer thickness and the distortion height are the same is $\epsilon = Re^{-\frac{1}{7}}$. In the linearized case ($H \ll 1$) a solution is found using Fourier transforms, so that if

$$\bar{A}(k) = \frac{1}{\sqrt{2\pi}} \int_{-\infty}^{\infty} e^{ikX} A(X)\, dX,$$

then, after solving for the wall layers which occur for $y = O(\epsilon^2)$ and $1-y = O(\epsilon^2)$, the unknown function $A(X)$ is given by

$$\bar{A}(k) = -\frac{H\bar{F}(k)}{2(1-\zeta(ik)^{\frac{7}{3}})},$$

where
$$\zeta = -\frac{\int_0^\infty \mathrm{Ai}\,(t)\, dt}{\mathrm{Ai}'\,(0)} = 1.2879,$$

and we require $-\frac{3}{2}\pi < \arg k < \frac{1}{2}\pi$ for the solution to exist. The displacement function is a convolution of $F(X)$ with a function whose transform is $1/(1-\zeta(ik)^{\frac{7}{3}})$.

There are three poles which satisfy the condition $-\frac{3}{2}\pi < \arg k < \frac{1}{2}\pi$. Smith (1976*b*) gave only the pole at $k = i\zeta^{-\frac{3}{7}}$; the other two poles are at $k = \zeta^{-\frac{3}{7}} e^{5\pi i/14}$ and

$k = \zeta^{-\frac{3}{7}}\,\mathrm{e}^{-19\pi\mathrm{i}/14}$. Upstream the pole at $k = -\mathrm{i}\zeta^{-\frac{3}{7}}$ gives an exponential decay of order $\exp(\zeta^{-\frac{3}{7}}X)$. Downstream there are two contributions, one from an integral on the branch cut whose large-X behaviour is $O(X^{-\frac{11}{3}})$ and the second coming from the two poles in the upper half-plane whose behaviour is like

$$\exp\left[-(\cos\tfrac{1}{7}\pi)\,\zeta^{\frac{3}{7}}x\right]\cos\left[(\sin\tfrac{1}{7}\pi)\,\zeta^{\frac{3}{7}}x+\tfrac{1}{7}\pi\right],$$

where we recall that $X = Re^{\frac{1}{7}}x$. Thus there is indeed a wavelike structure in the steady solution although it decays exponentially downstream. Sobey (1983) has shown that for intermediate Strouhal number during a deceleration a separated region will expand. One must ask whether the wavelike structure found in the steady solution can grow during a deceleration. We also note that the wavelength is only weakly dependent on the Reynolds number (as $Re^{\frac{1}{7}}$) and that would agree with our observations. In the case of small-amplitude oscillations of the wall, Bogdanova & Ryzhov (1983) have explored the nature of Tollmien–Schlichting solutions to the unsteady free-interaction boundary layers which exist on each wall. Their results are extremely interesting for they have found that as the frequency of the wall oscillation increases a neutrally damped wave occurs downstream of the section of moving wall at a critical frequency. This appears to agree closely with our observations and, if correct, would indicate that the genesis of a vortex wave is a damped Tollmien–Schlichting wave which the free-interaction equations can support.

Unfortunately, if we examine the scaling used by Bogdanova & Ryzhov we are given reason to pause. Their critical frequency parameter is, in our terms, $2\pi\,Re^{\frac{2}{7}}\,St \sim 5$. This predicts that as the Strouhal number is decreased the frequency at which a neutrally damped wave occurs will increase. In particular for a Strouhal number of 0.002 the critical frequency would be near 9000 Hz whereas we observed the neutrally damped wave at about 2 Hz. Our observations are also that as the Strouhal number decreases the Reynolds number for a neutrally damped wave also decreases. This suggests, but does not prove, that the genesis of the vortex wave does not come from the free-interaction boundary-layer equations.

An alternative description of vortex waves was proposed in I. That theory was a long wavelength one and was somewhat *ad hoc* but nevertheless several important features of the vortex wave were accurately predicted. In the appendix we extend the theory of I to account for varying flux through a rigid-walled channel. We derive a linearized Korteweg–de Vries equation as in I but with non-constant coefficients. Thus the theory of I can also be applied to our observations. If the longitudinal lengthscale is λ, where $1 \ll \lambda \ll Re$, the time parameter in the theory is $\lambda^3\,St$. We note that the theory of I does not predict a neutrally damped wave as the frequency increases and that an extension of that theory to include viscous effects is needed to obtain agreement with our observations.

There is no theory which completely describes the vortex wave. We believe that the results of Bogdanova & Ryzhov are very exciting, for they predict a neutrally damped wave. That they do not seem to apply to the experiments may not be so important. This is because their theory may be valid for very small Strouhal numbers where the Reynolds number needed to produce a wave may be asymptotically large as $St \rightarrow 0$. These waves are of Tollmien–Schlichting type and arise within the boundary-layer regions adjacent to each wall. As the Strouhal number is increased to an intermediate value, new effects become important and it is at this stage that a vortex wave is observed. The genesis of this wave does not come from within the viscous wall layers, but as the theory of I indicates it is inviscid interactions within the core flow which produce the wave. Further, in this region of intermediate Strouhal numbers the critical Reynolds number for the onset of the wave may increase as the Strouhal number is increased. Since our observations are in the later region our results would not then contradict the asymptotic theory. We also know that no asymptotic description of intermediate Strouhal number flow has yet emerged and for this region the best we can achieve may be along the lines of the *ad hoc* theory of I. Further numerical solutions, both of the nonlinear boundary-layer equations and the full Navier–Stokes equations, will shed considerable light on how a vortex wave can be generated and on unsteady separation.

Appendix. Description of inviscid core flow

The theory presented in I showed that during oscillations of a channel wall vortex waves could be described by a linearized Korteweg–de Vries equation. The description was obtained by neglecting the viscous wall layers and examining inviscid disturbances of sufficiently long wavelength. The analysis can be carried out because the undisturbed velocity profile is parabolic. Critical layers occur at the walls and their location means that viscous effects are not important at the level for which inviscid disturbances occur. We show here that the theory of I can be extended to the case of unsteady flow through a rigid-walled channel.

Suppose that far upstream the channel has width $2h$ and that variation of the channel width occurs over a length λh. An incompressible fluid of density ρ and viscosity ν flows through the channel with flux $\hat{q} = 2hUq(\Omega\hat{t})$. The coordinates, pressure and velocities are non-dimensionalized by

$$(\hat{x}, \hat{y}, \hat{t}, \hat{p}, \hat{u}, \hat{v}) \sim (\lambda hX, hy, \Omega^{-1}t, \rho U^2 p, Uu, \delta Uv),$$

where we define

$$\delta = \lambda^{-1}.$$

The equations of motion are

$$u_x + u_y = 0,$$

$$\lambda\, St\, \frac{\partial u}{\partial t} + uu_x + vu_y = -p_x + \lambda\, Re^{-1}\, \nabla^2 u,$$

$$\delta\, St\, \frac{\partial u}{\partial t} + \delta^2(uv_x + vv_y) = -p_y + \delta\, Re^{-1}\, \nabla^2 u,$$

where

$$\nabla^2 = \frac{\partial^2}{\partial y^2} + \delta^2 \frac{\partial^2}{\partial x^2}.$$

The boundary conditions are that, far upstream, u, v, and p are prescribed and that the flux through the channel is given by the function $q(t)$. The unperturbed flow, given by $u = U_0(y,t)$, $v = 0$, and $p = \lambda\, Re^{-1}\, xp_0(t)$, is the solution of

$$Re\, St \frac{\partial U_0}{\partial t} = -p_0(t) + \frac{\partial^2 U_0}{\partial y^2},$$

together with the boundary conditions

$$U_0(0,t) = U_0(1,t) = 0,$$

and

$$\int_0^1 U_0(y,t)\, \mathrm{d}y = q(t).$$

Assume that the velocities are described by a stream function ψ,

$$u = \psi_y \quad \text{and} \quad v = -\psi_x,$$

and for $\delta \ll 1$ expand

$$\psi \sim \psi_0 + \delta^2\psi_1 + \delta^4\psi_2 + \dots,$$

$$p \sim \lambda\, Re^{-1} x p_0(t) + \delta^4 p_1 + \dots.$$

The pressure scaling is required by $\partial p/\partial y = O(\delta^4)$. Assume that the walls are $y = \delta^2 F(X)$ and $y = 2 - \delta^2 G(x)$, so that the boundary conditions are

(i) $$\psi_0|_{y=0} = 0, \quad \psi_0|_{y=2} = q(t),$$

(ii) $$\psi_1|_{y=0} = -F\frac{\partial\psi_0}{\partial y}\bigg|_{y=0}, \quad \psi_1|_{y=2} = G\frac{\partial\psi_0}{\partial y}\bigg|_{y=2},$$

and

(iii) $$\psi_2|_{y=0} = -F\frac{\partial\psi_1}{\partial y}\bigg|_{y=0} - \tfrac{1}{2}F^2\frac{\partial^2\psi_1}{\partial y^2}\bigg|_{y=0}, \quad \psi_2|_{y=2} = G\frac{\partial\psi_1}{\partial y}\bigg|_{y=2} - \tfrac{1}{2}G^2\frac{\partial^2\psi_1}{\partial y^2}\bigg|_{y=2}.$$

Assuming as in I that $1 \ll \lambda \ll Re$, the first-order solution is

$$\psi_1 = A(X,t)\, U_0(y,t)$$

and

$$p_1 = p_{10}(X,t) + A_{xx}(X,t)\int_0^y U_0^2(s_1 t)\,\mathrm{d}s.$$

The second-order stream function satisfies the equation

$$\delta^{-3} St\,(A_t U_{0y} + A U_0 t_y) + A A_x (U_{0y}^2 - U_0 U_{0yy}) + U_0 \psi_{2xy} - U_{0y}\psi_{2x} = -p_{10}(x_1 t) - A_{xxx}\int_0^y U_0^2(s,t)\,\mathrm{d}s,$$

and if we let $\omega = \delta^{-3} St \sim O(1)$ then:

$$\psi_{2x} = -A A_x U_{0y} + \omega\left(A_t - A U_0 \int_1^y \frac{U_{0st}}{u_0^2}\,\mathrm{d}s\right) - p_{10} U_0 \int_1^y \frac{\mathrm{d}s}{U_0^2} - A_{xxx} U_0 \int_1^y \frac{\int_0^p U_0^2(s,t)\,\mathrm{d}s}{U_0^2(p,t)}\,\mathrm{d}p + U_0 B(x,t),$$

where $B(x,t)$ is an unknown function.

If we let

$$a(t) = \left(U_0 \int_1^y \frac{U_{0st}}{U_0^2}\,\mathrm{d}s\right)\bigg|_{y=2} + \left(u_0 \int_1^y \frac{U_{0st}}{U_0^2}\,\mathrm{d}s\right)\bigg|_{y=0},$$

$$b(t) = \left(U_0 \int_1^y \frac{\int_0^p U_0^2(s,t)\,\mathrm{d}s}{U_0^2(p,t)}\,\mathrm{d}p\right)\bigg|_{y=2},$$

and

$$\sigma = U_{0y}|_{y=0},$$

the boundary conditions give

$$bA_{xxx} - \omega(2AA - aA) = \sigma\{[(F+G)A]_x + FF_x - GG_x\}.$$

This equation is analogous to that obtained in I except that the coefficients a and b are now time dependent.

This work was supported by the SERC. I am grateful to Mr J. Strange for building the experimental apparatus and to Dr T. J. Pedley, Dr S. Cowley, Dr O. Tutty and Mr M. Borgas for many fruitful discussions.

REFERENCES

ARMALY, B. F., DURST, F., PEREIRA, J. & SCHONUNG, B. 1983 *J. Fluid Mech.* **127**, 473–496.

BERTRAM, C. D. & PEDLEY, T. J. 1982 *J. Fluid Mech.* **130**, 315–345.

BOGDANOVA, E. V. & RYZHOV, O. S. 1983 *Q. J. Mech. Appl. Maths* **36**, 271–287.

CHERDRON, W., DURST, F. & WHITELAW, J. H. 1978 *J. Fluid Mech.* **84**, 13–31.

COWLEY, S. J. 1981 Ph.D. thesis, University of Cambridge.

DENHAM, M. K. & PATRICK, M. A. 1974 *Trans. Inst. Chem. Engng* **52**, 361–367.

DUCK, P. 1984 *Q. J. Mech. Appl. Maths* (in the press).

DURST, F., MELLING, A. & WHITELAW, J. H. 1974 *J. Fluid Mech.* **64**, 111–128.

GOLDSTEIN, R. J., ERIKSON, V. L., OLSEN, R. M. & ECKERT, E. R. G. 1970 *Trans. ASME* D: *J. Basic Engng* **92**, 732–740.

JOHN, P. 1984 Ph.D. thesis, University of London.

SECOMB, T. 1979 Ph.D. thesis, University of Cambridge.

SMITH, F. T. 1976*a* *Q. J. Mech. Appl. Maths* **29**, 343–364.

SMITH, F. T. 1976*b* *Q. J. Mech. Appl. Maths* **29**, 365–376.

SMITH, F. T. 1977 *J. Fluid Mech.* **90**, 727–753.

SMITH, F. T. & DUCK, P. 1980 *J. Fluid Mech.* **98**, 727–753.

SOBEY, I. J. 1980 *J. Fluid Mech.* **96**, 1–26.

SOBEY, I. J. 1982 *J. Fluid Mech.* **125**, 359–373.

SOBEY, I. J. 1983 *J. Fluid Mech.* **134**, 247–257.

STEPHANOFF, K. D., PEDLEY, T. J., LAWRENCE, C. J. & SECOMB, T. W. 1983 *Nature*, **305**, 692–695.

TERENTEV, E. D. 1981 *Prikl. Math. Mech.* **45**, 1049–1055.